Louisiana State University
LSU Digital Commons

LSU Master's Theses | Graduate School

2015

Characterization of Biopolymer using SWCC and Microfluidic Models: Implication on EOR

Jungyeon Jang
Louisiana State University and Agricultural and Mechanical College, jjang2@lsu.edu

Follow this and additional works at: https://digitalcommons.lsu.edu/gradschool_theses

 Part of the Civil and Environmental Engineering Commons

Recommended Citation
Jang, Jungyeon, "Characterization of Biopolymer using SWCC and Microfluidic Models: Implication on EOR" (2015). *LSU Master's Theses*. 3671.
https://digitalcommons.lsu.edu/gradschool_theses/3671

This Thesis is brought to you for free and open access by the Graduate School at LSU Digital Commons. It has been accepted for inclusion in LSU Master's Theses by an authorized graduate school editor of LSU Digital Commons. For more information, please contact gradetd@lsu.edu.

CHARACTERIZATION OF BIOPOLYMER USING SWCC AND MICROFLUIDIC MODELS: IMPLICATION ON EOR

A Thesis

Submitted to the Graduate Faculty of the
Louisiana State University and
Agricultural and Mechanical College
in partial fulfillment of the
requirements for the degree of
Master of Science in Civil Engineering

in

The Department of Civil and Environmental Engineering

by
Jungyeon Jang
B.S., Konkuk University, 2009
August 2015

ACKNOWLEDGMENTS

First of all, I am a very pleased to study at Louisiana State University with distinguished professors. I still cannot believe how I could purse a master degree program in Civil Engineering at LSU. This incredible opportunity has given me the opportunity to concentrate on geotechnical engineering. Pursuing a graduate degree in the United States has been challenging and time-consuming, but it is truthfully a worthwhile experience for my whole life.

On top of that, I would like to thank Dr. Jongwon Jung with his enormous guidance, understanding, patience, and opportunity for me as one of his research group members. He has provided a geotechnical laboratory without any hesitation for me and has always been a perfect mentor with his paramount passion for his research. Moreover, I sincerely appreciate Dr. Mostafa Elseifi and Dr. Shengli Chen for being members of my committees. I would like to thank Dr. Mostafa Elseifi for his deliberative advice. I would like to thank Dr. Shengli Chen for giving me cheering comments as well.

Lastly, I dedicate this thesis to my lovely wife, Mihye Oh, whose had endless love and support for me since I decided to study in the United States. Furthermore, I would like to thank my parents for their unlimited patience: My mother, Hye-Lan Seo who always trusts in me without doubt, and my respectful father, Hak-Sung Jang, who gave me incredible talents. Last but not least, I would like to thank my influential supporters in South Korea: Dr. Hee-Chang Lee, Dr. Kee-Won Seong, Dr. Dong-Ho Ha, and Dr. Jinkyo Choo.

TABLE OF CONTENTS

ACKNOWLEDGMENTS ii

LIST OF TABLES v

LIST OF FIGURES vi

NOTATION x

ABSTRACT xi

CHAPTER 1. INTRODUCTION 1
1.1. Background 1
1.2. Problem Statement 2
1.3. Objective 2
1.4. Scope 3
1.5. Outline 3

CHAPTER 2. LITERATURE REVIEW 4
2.1. Biopolymers 4
2.1.1. Origin 4
2.1.2. Types 6
2.1.3. Structure 6
2.1.4. Soil Stabilization 7
2.1.5. Enhanced Oil Recovery (EOR) 8
2.2. Multiphase Fluids Flow 10
2.2.1. Two Fluids Displacement 10
2.2.2. Viscosity 12
2.2.3. Contact Angle 16
2.2.4. Surface Tension 18
2.3. Soil-Water Characteristic Curve (SWCC) 19
2.3.1. Capillary Pressure: Drain – Imbibition Curve 20

CHAPTER 3. EXPERIMENTAL PROCEDURES 24
3.1. Materials 24
3.2. Viscosity 25
3.3. Contact Angle 27
3.4. Surface Tension 28
3.5. Microfluidic Models 29
3.6. Soil-Water Characteristic Curve (SWCC) 34

CHAPTER 4. EXPERIMENTAL RESULTS 39
4.1. Viscosity 39
4.2. Contact Angle 42
4.3. Surface Tension 44

4.4. Microfluidic Models....45
4.5. Soil-Water Characteristic Curve (SWCC)....47

CHAPTER 5. ANALYSES AND DISCUSSION....49
5.1. Analyses and Discussion....49
5.2. Estimate of Capillary Pressure using *e, Cc, and Ss*....56
5.3. Effective Stress on the Capillary Pressure....57

CHAPTER 6. CONCLUSIONS AND FUTURE WORK....59
6.1. Conclusions....59
6.2. Future Work....60

REFERENCES....61

APPENDIX A: CONTACT ANGLES OF DISTILLED WATER, AGAR, AND PAM IN THE AIR, HEXADECANE....66

APPENDIX B: THE FLOW PATTERN USING PAM SOLUTIONS IN THE HEXADECANE....75

VITA....78

LIST OF TABLES

Table 3.1 The basic soil parameters of Ottawa sand F-75 25

Table 3.2 Test plans of the viscosity of Agar and PAM solutions with different concentrations and temperatures using Brookfield viscometer (DV-III) 26

Table 3.3 The implements of distilled water and Agar/PAM solutions in the air/hexadecane for Microfluidic models 34

Table 3.4 The properties of Ottawa sand F-75 and 0.5-bar ceramic stone 36

Table 3.5 The properties of four chambers for SWCC test 37

Table 4.1 The properties of Brookfield viscometer (DV-III) 39

LIST OF FIGURES

Figure 2.1 Basic chemical structures of Agar (Lahaye and Rochas 1991) 6

Figure 2.2 The structure of Nonionic polyacrylamide (PAM) (Barvenik 1994).....7

Figure 2.3 Displacement aspects of the relationship between log C and M. (a) Viscous fingering. (b) Stable displacement. (c) Capillary fingering (Lenormand 1990; Sinha and Wang 2007).....11

Figure 2.4 Flow curves of Newtonian and non-Newtonian fluids. (a) Correlation between shear rate and stress. (b) The relationship between shear rate and viscosity 13

Figure 2.5 Each curve of shear-thinning fluid as a function of shear rate depends on (a) Shear stress. (b) Apparent viscosity. 14

Figure 2.6 Each curve of shear-thickening fluid as a function of shear rate depends on (a) the shear stress and (b) the apparent viscosity.....15

Figure 2.7 Definition of the relationships between interfacial tension, capillary pressure, and contact angle (Weisbrod et al. 2002) 16

Figure 2.8 Typical soil-water characteristic curves for silt soil (Fredlund and Xing 1994).....22

Figure 2.9 Typical soil-water characteristic curves for sandy soil, silt soil, and clayey soil (Fredlund and Rahardjo 1993).....22

Figure 3.1 Particle-size distribution curves of Ottawa F-75 and sand for sieve analysis.....24

Figure 3.2 Brookfield viscometer model DV-III. (a) A picture in the lab. (b) A schematic design.....26

Figure 3.3 The representative images of contact angle with a SiO_2 surface. (a) - (b) contact angles in the air. (c) - (d) contact angles in Hexadecane. (b) and (d) are shown by measuring the contact angle using ImageJ 1.48 software.....27

Figure 3.4 Measurement of the surface tension of biopolymers using Sigma 703D force tensiometer. (a) Setup for a test. (b) During the test.....28

Figure 3.5 The components of the microfluidic models. (a) Chipholder kit. (b) A setup of chip holder and an enlarged microfluidic chip. (c) The microfluidic chip 30

Figure 3.6 The experimental setup for microfluidic models 31

Figure 3.7 The schematic designs of the experimental setup for Microfluidic models. (a) Testing. (b) Flushing and cleaning. 32

Figure 3.8 The setup of SWCC tests. (a) In the lab. (b) The schematic design 35

Figure 3.9 The pictures of SWCC tests. (a) A chamber (b) the setting chamber with sand and water (c) the setup of SWCC tests prior to the experiment.....36

Figure 4.1 Effect of temperature on viscosity: (a) 0.2g/L Agar, (b) 2g/L PAM, (c) 5g/L PAM, (d)10g/L PAM, (e) 15g/L PAM, (f) 20g/L PAM solutions using the Brookfield viscometer (DV-III).....41

Figure 4.2 The effect of different concentration of Agar and PAM solutions on contact angle, compared with distilled water: (a) In the air. (b) In the hexadecane.....43

Figure 4.3 Surface tensions of 0.2g/L Agar and PAM solutions at the room temperature (25 ℃) 44

Figure 4.4 The effect of PAM solutions using microfluidic models on pore saturation in the Hexadecane depends on (a) flow rate on a log scale (b) its concentration 46

Figure 4.5 The calibration of each chambers using distilled water for capillary pressure (a) as a unit of cmH_2O, (b) kPa.....47

Figure 4.6 The Pc-Sw relationships of distilled water with four chambers: (a) No. 1 and No. 2. (b)No. 3 and No. 4.....48

Figure 4.7 Pc-Sw relationships of 2g/L PAM solution with chamber No.2 and No. 4.....48

Figure 5.1 The correlation between pore saturation and Log M (mobility ratio) of Agar solutions (2, 5, 10, 15, 20g/L) at room temperature (25℃) in the air. (a) 0.3µl/min. (b) 1.0µl/min. (c) 50µl/min.(d) 50µl/min in details.....51

Figure 5.2 The correlation between pore saturation and Log C (Capillary number) of Agar solutions (2, 5, 10, 15, 20g/L) at room temperature (25℃) in the air. (a) 0.3µl/min. (b) 1.0µl/min. (c) 50µl/min. (d) 50µl/min in details 52

Figure 5.3 The correlation between the mobility ratio (M) and the Capillary number (C) of distilled water and Agar solutions (2, 5, 10, 15, 20g/L) at room temperature (25℃) in the air 53

Figure 5.4 The correlation between pore saturation and (a) the mobility ratio (M) and (b) the capillary number (C) of distilled water and PAM solutions (2, 5, 10, 15, 20g/L) at room temperature (25℃) in the air 53

Figure 5.5 The correlation between the mobility ratio (M) and the Capillary number (C) of distilled water and PAM solutions (2, 5, 10, 15, 20g/L) at room temperature (25℃) in the air 54

Figure 5.6 The correlation between pore saturation of various PAM solutions in the hexadecane as a function of (a) Mobility ratio (M) and (b) Capillary number (C) 55

Figure 5.7 Correlation of PAM solutions with a different concentration of the mobility ratio (M) and the Capillary number (C) at room temperature in the hexadecane 56

Figure 5.8 Capillary pressure in sediments as a function of depth for different sediment mineralogies using each average values: Silt (e_{100} = 0.7, Cc = 0.06, Ss = 0.5225m^2/g), Kaolinite (e_{100} = 1.0, Cc = 0.3, Ss = 15m^2/g), Illite (e_{100} = 2.5, Cc = 0.8, Ss = 82.5m^2/g), Montmorillonite (e_{100}= 3.25, Cc = 1.5, Ss = 540m^2/g).....57

Figure 5.9 Estimate of capillary pressure (Max, Average, Min) in sediments as a function of effective stress (MPa) for different sediment mineralogies: (a) Silt (e_{100} = 0.6 – 0.8, Cc = 0.02 *0.09, Ss = 0.05 – 1.0 m^2/g), (b) Kaolinite (e_{100} = 0.9 – 1.1, Cc = 0.2 – 0.4, Ss = 10 -20m^2/g), (c)Illite (e_{100} = 2 - 3, Cc = 0.8 - 80, Ss = 65 - 100m^2/g), (d) Montmorillonite (e_{100} = 3.25, Cc = 1.5, Ss= 300 - 780m^2/g) 58

Figure A.1 Analyses of distilled water on contact angle using ImageJ software in the air.....66

Figure A.2 Analyses of Agar using ImageJ software on contact angle in the air. (a) 2g/L Agar (b) 5g/L Agar (c) 10g/L Agar (d) 15g/L Agar (e) 20g/L Agar 67

Figure A.3 Analyses of PAM using ImageJ software on contact angle in the air. (a) 2g/L PAM (b) 5g/L PAM (c) 10g/L PAM (d) 15g/L PAM (e) 20g/L PAM.....69

Figure A.4 Analyses of distilled water using ImageJ software on contact angle in the Hexadecane 70

Figure A.5 Analyses of Agar using ImageJ software on contact angle in the Hexadecane. (a) 2g/L Agar (b) 5g/L Agar (c) 10g/L Agar (d) 15g/L Agar (e) 20g/L Agar 71

Figure A.6 Analyses of PAM using ImageJ software on contact angle in the Hexadecane. (a) 2g/L PAM (b) 5g/L PAM (c) 10g/L PAM (d) 15g/L PAM (e) 20g/L PAM.....73

Figure B.1 Displacement patterns of distilled water as a function of the flow rate on Microfluidic models in the Hexadecane 75

Figure B.2 Displacement patterns of 2g/L PAM as a function of the flow rate on Microfluidic models in the Hexadecane 75

Figure B.3 Displacement patterns of 5g/L PAM as a function of the flow rate on Microfluidic models in the Hexadecane 76

Figure B.4 Displacement patterns of 10g/L PAM as a function of the flow rate on Microfluidic models in the Hexadecane 76

Figure B.5 Displacement patterns of 15g/L PAM as a function of the flow rate on Microfluidic models in the Hexadecane 77

Figure B.6 Displacement patterns of 20g/L PAM as a function of the flow rate on Microfluidic models in the Hexadecane 77

NOTATION

AEV	Air-Entry Value
C	Capillary Number
P_c	Capillary pressure
S_w	Degree of Saturation
EOR	Enhanced Oil Recovery
σ	Interfacial tension
M	Mobility ratio
PAM	Polyacrylamide
SWCC	Soil-Water Characteristic Curve
V	The velocity of non-wetting phase
μ_{nw}	The viscosity of the non-wetting phase
μ_w	The viscosity of the wetting phase

ABSTRACT

The objective of this study is to investigate the characteristics of biopolymers and to examine their application for soil stabilization and oil production. Biopolymers, the composite of multi-living organisms, are one of the most promising materials in the field of geotechnical engineering. The application of biopolymer is more efficient than water for soil stabilization and oil production due to its higher viscosity as a fill material of pores in the soil.

This thesis begins with a definition of Agar and Polyacrylamide (PAM) as the measurement of viscosity, contact angle, and surface tension. The application of microfluidic models are applied to perceive the flow of liquids in porous media for Enhanced Oil Recovery (EOR) techniques. The result of using microfluidic models is that the displacement ratio (range: 12.9 ~ 39.6%) of PAM solutions is higher than distilled water at the flow rate of 0.001ml/min. Soil-Water Characteristic Curve (SWCC) tests are conducted to interpret the property of biopolymers for soil stabilization. The results of the SWCC tests using biopolymers show that the capillary pressure with biopolymers is higher than distilled water in sandy soils. Therefore, the applications of biopolymer are more efficient than distilled water for soil stabilization.

CHAPTER 1. INTRODUCTION

1.1. Background

Over recent decades, Biopolymers, called “living organisms,” are one of the most promising materials for the whole industry, as well as in the field of geotechnical engineering (Chandra and Rustgi 1998). In many papers, the application of biopolymers has influenced for soil remediation and oil production for Enhanced Oil Recovery (EOR) techniques. Due to its stability and eco-friendliness with the increase of concerns about environmental issues, the biopolymer is one of the most future-oriented ways in any field, as well as the area of geotechnical engineering.

The biopolymer is still unfamiliar, associated with researchers and workers in the field of geotechnical engineering. Many previous papers, written by scientists from chemical engineering or chemistry departments, have mostly focused on how the molecular structures of biopolymers change or combine with each other, rather than their application. However, we need to investigate biopolymers to examine the usages for soil remediation and oil productions. We also focus on fluid flow in porous media for them. Therefore, we would evaluate what the characteristics of biopolymers are and how they can effectively apply to the field of geotechnical engineering.

In this study, Agar and Polyacrylamide (PAM) are used to evaluate their characteristics for soil remediation and oil productions. To prove it, we have conducted the significant tests: Soil-Water Characteristic Curve (SWCC) and Microfluidic models. The lower surface tension of the PAM solution may enable the contaminated water in the ground to easily be expelled at the point of its Air-Entry Value (AEV) through SWCC tests. The higher displacement ratio of the PAM

solution may obtain more crude oil than distilled water using microfluidic models. Therefore, the potential characterization of biopolymers may be efficient for soil remediation and oil production.

1.2. Problem Statement

Though many research papers have evaluated the properties of biopolymers and their application for soil remediation or EOR techniques, none of them has adopted the particular application of Agar and PAM. After the characterization of Agar and PAM through SWCC and Microfluidic models are defined, we discuss implications of Agar and PAM on soil remediation and EOR techniques.

1.3. Objective

The ultimate aim of this study is to evaluate if the usage of Agar and PAM as biopolymers is beneficial for soil remediation and EOR methods. To interpret the distinguished properties of Agar and PAM (2,5,10,15,20g/L), we have conducted three fundamental tests (Contact angle, Viscosity, and Surface tension tests) and two outstanding tests (SWCC and Microfluidic models) with Agar and PAM.

The characterization of Agar and PAM through SWCC and Microfluidic models is supported by their results. In the SWCC tests, we evaluate how biopolymers affect the capillary pressure in the same soil conditions, and then their effect may give a huge impact on soil stabilization. Microfluidic models with Agar and PAM explain how biopolymers added to water can improve oil production from an oil reservoir through a higher displacement ratio of PAM, rather than distilled water on EOR techniques. After obtaining outcomes from these tests, it is highly reliable to apply biopolymers for soil stabilization and EOR techniques.

1.4. Scope

The main scope of this study consists of two distinguished types: short-term tests (contact angle, viscosity, and surface tension) and long-term tests (SWCC and Microfluidic models). To obtain the results of short-term tests, they are implemented carefully and repeatedly. Through the results of measuring contact angle and surface tension tests with the induced Young-Laplace equation, the values of capillary pressure are compared between directly and derived measured SWCC tests using the results of contact angle and surface tension. In order to distinguish the displacement patterns of Agar and PAM solutions, we measure their viscosity. The Microfluidic models are conducted to evaluate the displacement ratio of PAM in the hexadecane as assumed an oil reservoir as well.

1.5. Outline

This study composes of six chapters: Introduction, Literature review, Experimental methodology, Experimental results, Analyses & Discussion, and Conclusions and Future work. Chapter 1, Introduction, provides an overview of the study, stating the main problem that the study attempts to solve and introduce how to begin solving the problem. Following the introduction, chapter 2, the literature review, collects numerous studies which researchers have already conducted about the problem and tried to find out a better solution. Chapter 3, experimental methodology, is taken to conduct this study, and the laboratory testing is presented. Subsequently, chapter 4, experimental results, states the results of the laboratory testing. Chapter 5, analyses and discussion, discuss the laboratory data and evaluation in detail. Based on the analysis of the results obtained from this study, the conclusion chapter contains information on how we reached the scope of the study, how we could obtain a better outcome.

CHAPTER 2. LITERATURE REVIEW

2.1. Biopolymers

Biopolymers, called "natural polymers," are high polymers that are created by "living organisms" in nature (Chandra and Rustgi 1998). Biopolymers have the possibility to be cost-efficient in the oil industry due to their plugging effect in porous media, which reduces the permeability of soils (Martin et al. 1996). In addition, the applications of biopolymers can be potentially economical in the oil industry similar to the plugging effect of slime in porous media (Martin et al. 1996).

Agar and Polyacrylamide (PAM) are selected for this study. The process of selecting among countless biopolymers is highly important to find the best fit biopolymer, possibly enhances its mechanical properties (Busscher et al. 2009; Khatami and O'Kelly 2012). Agar and PAM are satisfactory for preventing soil loss with an eco-friendly property. Adding modified starch to Agar increases the cohesion and stiffness of the soil when Agar with adding modified starch increases cohesion and stiffness of the soil, compared to only agar at the same concentration, and agar is non-toxic to the environment (Khatami and O'Kelly 2012). The distinguished property of Agar is gel-forming that would modify strength (Praiboon et al. 2006). PAM has a specific property which is that when it is added to costal sands, it improves its mechanical properties (Busscher et al. 2009).

2.1.1. Origin

In this study, we select two major biopolymers: Agar and Polyacrylamide (PAM). Agar is usually obtained from specific seaweeds. First, Agar is taken from the agarose, which various

species of red algae include in the cell walls, and consists of mainly agarose and agaropectin (Khatami and O'Kelly 2012; Bornman and Barnard 1993). Agar would easily mix with hot water, and change to a gel when it is cooled (Bornman and Barnard 1993; Freile-Pelegrin et al. 2007). The manufacturing processes of agar consists of five main steps: Treatment, controlling, removal, need, and dehydrating steps (Armisen and Galatas 1987). The first step is called the alkaline treatment. This is one of the most important processes for the whole process due to the effects of degree conditions of Agar. Secondly, the molecular weight of agar is controlled when it is extracted with cold or boiling water. By variation of the molecular weight of agar, Agar's outputs are affected. In the third step, due to the previous extraction process, lots of secondary products are created alongside Agar. They should be eliminated or removed to obtain pure Agar. Fourthly, agar extracts are used during the manufacturing process to maintain a particular concentration range (0.8% to 1.5%) of agar when adding lots of water (Armisen and Galatas 1987). In order to obtain as much agar extracts as possible, their usage is necessary. Finally, pure agar extracts are collected from their mixed conditions. In the former process, lots of water are added to maintain the low concentration of agar. Diverse methods have developed in the industry such as evaporation, precipitation, freezing, and syneresis. After such methods are carefully applied, we can obtain pure agar extracts from seaweed.

Polyacrylamide (PAM) is defined in the terminology of chemistry (Sojka and Surapaneni 2000). Large amounts of PAM can be created by a chain length of each polymer and a variety type of materials with the string (Sojka and Surapaneni 2000). PAM consists of the polymerization of acrylamide subunits (Sojka et al. 2007; Ver Vers 1999; Kang et al. 2013). Asparagines and reducing sugars react with each other, and lots of Acrylamide, C_3H_5NO, is

created by the reaction, especially when starchy foods are baked or fried (Erkekoglu and Baydar 2014).

2.1.2. Types

Agar ($C_{12}H_{18}O_9$), powder by Alfa Aesar and PAM (Molecular Weight: 200,000), powder by ACROS Organics, are used in this study. The difference among various types of Agars is small. However, PAMs are different depending on their molecular weights.

Types of PAM include nonionic, cationic, and anionic, depending on its molecular weight (MW) (Barvenik 1994). Cationic PAMs are effective as flocculants for wastewater treatment processes (Barvenik 1994). Since 1995, anionic PAM is the most frequently used among them because it has an outstanding capacity for decreasing soil loss as a flocculant in agriculture, and has a much lower toxicity than nonionic and cationic PAMs (Sojka et al. 2007). Besides, anionic PAM is verified by the usage of the food industry (Sojka et al. 2007). These facts explain why PAM should be applied, depending on compatible situations among its various types. In this study, we decided to use PAM (MW 200,000, ACROS Organics).

2.1.3. Structure

The chemical structures of Agar and PAM are shown in Figure 2.1 and 2.2, respectively.

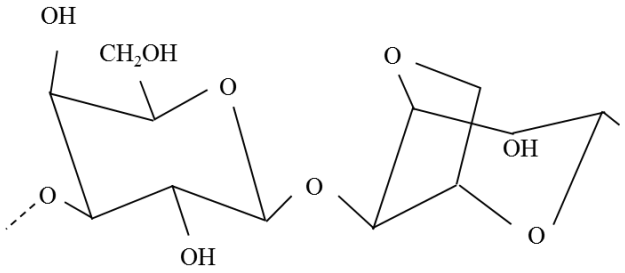

Figure 2.1. Basic chemical structures of Agar (Lahaye and Rochas 1991).

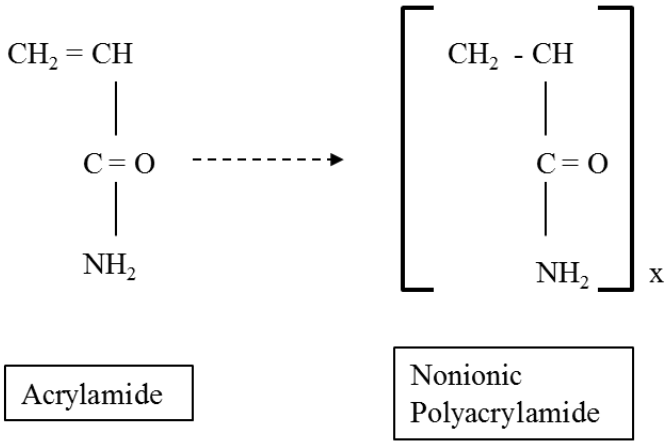

Figure 2.2. The structure of Nonionic polyacrylamide (PAM) (Barvenik 1994).

2.1.4. Soil Stabilization

Injection of biopolymers into the soil enhances soil stabilization by improving soil strength and reducing soil loss. Two different biopolymers, Agar and PAM in this study, also have such properties. Agar, one of the most popular biopolymers, is openly used for stabilizing soils due to its non-toxic. For example, Agar is postulated that cohesion intercepts of sand, from 0 to 245, dramatically are enhanced as an increment of its concentration (Khatami and O'Kelly 2013). Through unconfined compression tests, higher agar concentration increase more deviator stress with a treated sand more than an untreated sand (Khatami and O'Kelly 2013). Unlike an Agar solution and soil, adding modified starch with Agar is the largest cohesion compared to other conditions (Khatami and O'Kelly 2013). These previous results mean that the application of Agar for soil stabilization is very active and has potential.

PAM, another biopolymer in this study, improves soil stabilization for agricultural land, construction sites, canals, and pond sealings. The application of PAM in the agricultural industry prevents soil erosion through the reduction of soil particles (Sojka et al. 2007). For instance, an

application of a little PAM for irrigation prevents over 90% of soil losses from furrows, but only at the early part of runoff (Lentz and Sojka 1994). The application of either water-soluble anionic polyacrylamide (WSPAM) or PAM increase overall crop yields (Lentz and Sojka 2009; Sojka et al. 2006). Therefore, PAM prevents soil losses and promotes crop yields.

The PAM-treated irrigations reduce soil loss better than non-treated furrow ones (Lentz and Sojka 1994). The formulation of WSPAM significantly reduces soil losses (Lentz and Sojka 2009). Through the practical usage of PAM, it is a viable option for researchers and farmers due to its economical and eco-friendly properties (Sojka and Lentz 1997). In addition, using PAM is a very efficient way to prevent furrow irrigation-induced soil erosion. Farmers should carefully determine if full rate application is required for adequate control of their fields (Sojka and Lentz 1997). The PAM-treated irrigations might reduce soil loss better than non-treated furrow ones (Lentz and Sojka 1994). The application of PAM is a very powerful tool for preventing soil erosion in the field of agriculture (Kang et al. 2013). Moreover, even though PAM is an efficient and inexpensive way to prevent furrow irrigation-induced soil erosion for farmers, they should determine if full a rate application is required for adequate control of their fields (Sojka and Lentz 1997).

2.1.5. Enhanced Oil Recovery (EOR)

For several decades, numerous EOR studies have been conducted by many researchers in the oil field. EOR methods consist of two broad categories: thermal and non-thermal methods. In the latter, non-thermal EOR methods involve miscible, chemical, immiscible gas drives methods and so on. Thermal EOR methods are usually applied to heavy oil reservoirs, whereas non-thermal methods usually are employed for light oil reservoirs. Polymer injection, involving the

biopolymer injection technique, has primarily been concentrated on light oil reservoirs, and is also included by chemical methods (Khan and Islam 2007).

To increase the efficiency of oil production, many researchers in the oil field have looked forward to a better solution to gather more oil quantity from their reservoirs, rather than saving oil. Therefore, the most reliable answer is Enhanced Oil Recovery (EOR) methods, which means that the amount of oil production will be improved through the use of specific techniques.

CO_2 injection is one of the most famous techniques for EOR used over the years (Alvarado and Manrique 2010). CO_2 injection is applied by injecting carbon dioxide into oil reservoirs to gather residual oil between rock pores and air. Due to this procedure, the amount of CO_2 in the air is reduced. CO_2 injection has also solved environmental issues. On the other hand, the storage of CO_2 after injecting CO_2 into the soil remains a complicated problem that awaits us. Due to insufficient infrastructures and knowledge, CO_2 injection is an unclear solution for EOR. Biopolymer flooding has continuously developed to be a better solution for EOR. Improving biopolymer flooding obtains the best fit to recover as much oil production as possible using reservoir simulation and modeling.

Biopolymer flooding is more potential than outdated methods such as the CO_2 injection method on EOR. Polymer flooding has been applied for more than half a century, and its fundamental principle is to mobilize displacement between oil and water (Standnes and Skjevrak 2014). Biopolymer flooding is one of the polymer flooding techniques for EOR. The fact is verified by the developed biopolymer flooding due to encountered limitations. The feasibility of biopolymer flooding for EOR is very positive because many researchers have continuously been studying the implications of biopolymer flooding.

Biopolymer flooding, originated by polymer flooding in EOR, has targeted a niche market in the oil field. Injecting biopolymers is very difficult because biopolymer flooding perfectly substitutes for existing petroleum-based plastics. Through non-toxic decomposition of the biopolymer in the ground, biopolymer flooding focuses on the environmental aspect rather than solely polymer flooding.

2.2. Multiphase Fluids Flow

2.2.1.Two Fluids Displacement

The dispersed patterns of two immiscible fluids in porous media plays an important role in estimating how to transport (Lenormand 1990). In this study, two immiscible displacements are considered as a drainage process using Microfluidic models. Two Immiscible Fluids in porous media are affected by viscous pressure and capillarity (Lenormand 1990; Sinha and Wang 2007). The three main dispersed patterns are proposed shown in Figure 2.2: viscous fingering, stable displacement, and capillary fingering (Lenormand 1990). These patterns are determined by C, the capillary number, and M, mobility ratio (Lenormand 1990; Sinha and Wang 2007):

$$C = V\mu_{nw} / \sigma \tag{2.1}$$

$$M = \mu_{nw} / \mu_{w} \tag{2.2}$$

where V = the velocity of non-wetting phase

μ_{nw} = the viscosity of the non-wetting phase

μ_{w} = the viscosity of the wetting phase

σ = the interfacial tension.

The parameters, C and M, play an important role in distinguishing the displacement aspects of the wetting and non-wetting phases shown in Fig 2.3. C, Capillary number, means that viscous forces are divided by capillary forces (Romero-Zeron 2012). Also, M, viscosity ratio, is related to the viscosity of wetting and non-wetting liquids.

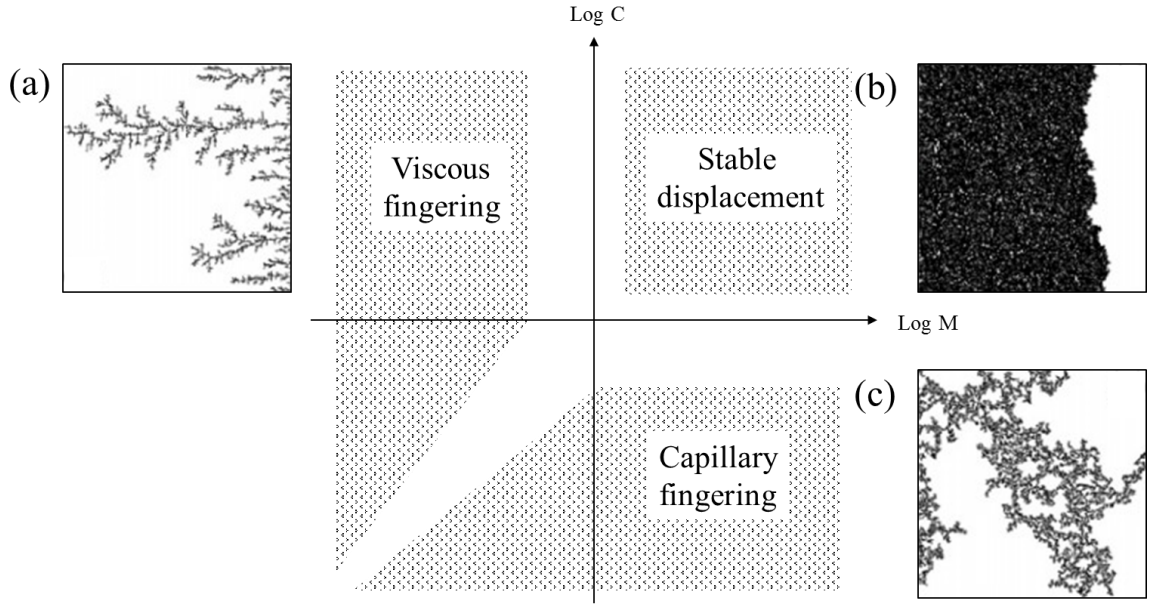

Figure 2.3. Displacement aspects of the relationship between log C and M. (a) Viscous fingering. (b) Stable displacement. (c) Capillary fingering (Lenormand 1990; Sinha and Wang 2007).

With the capillary number (C) and viscosity ratio (M), Agar and PAM are distinguished as two parts: unstable displacement (Viscous fingering, capillary fingering) and stable displacement. The fundamental cause of fingerings is the difference of viscosity between two Immiscible Fluids in porous media shown in Fig 2.2. The determination of viscous fingering depends on the viscosity of both a wetting phase and a non-wetting phase. Minute discontinuous water droplets at the oil/water interface are very efficient to decrease viscous fingering effects (Du et al. 2013). Capillary fingering is affected by the injecting speed of non-wetting phases with

the capillary number (C) when it is small. Even though the two distinguished fingerings are difficult to understand in porous media, we should try to evaluate them due to the characterization of biopolymers.

2.2.2. Viscosity

Viscosity is one of the most important properties for enhancing oil recovery, even in unsaturated soil mechanics. The definition of viscosity is the resistant capacity of fluid to flow (Elert 1998). Viscosity consists of dynamic viscosity and kinematic viscosity. The common unit of dynamic viscosity is the dyne second per square centimeter (dyn-s/cm^2), which is given the name poise (P) (Elert 1998). Additionally, it is performed by the following:

1 Pa·s = 10 poise = 1,000 mPa·s, 1cP=1mPa·s

The SI unit of viscosity is the Pascal second (Pa s), but it is rarely used in scientific and technical publications.

A typical unit of kinematic viscosity is the square centimeter per second (cm^2/s), which is given the name stokes (St). It is showed by the following:

1m^2/s= 10,000 cm^2/s (stokes) = 1,000,000mm^2/s (centistokes)

1 cm^2 /s = 1 stokes, 1mm^2 /s = 1 centistokes

The viscosity of liquids only depends on temperature and pressure. Viscosity varies with temperatures such as honey, syrups, and engine oil. For instance, the viscosity of water at 20 Celsius is 1.0020 millipascal seconds. Also, the viscosity of oil machine as light 20 degrees and massive 20 degrees are 102cP.

The measurement of viscosity has four different distinguished methods, consisting bubble viscometers, flow cups, dip cups and rotational viscometers. Among these methods, this study uses rotational viscometers.

Newtonian Fluid is not affected by the shear rate, called injection speed, because its viscosity maintains constant, such as water and air (Fimmtech 2007). On the other hand, Non-Newtonian fluid is mostly affected by the injection speed. Unlike Newtonian fluid, the viscosity depends on the shear rate and may be changed; such as, salt solutions and molten polymers (Fimmtech 2007). Pseudoplastic, referred to as shear thinning, is when the apparent viscosity decreases with increased stress, such as ketchup, blood, and nail polish.

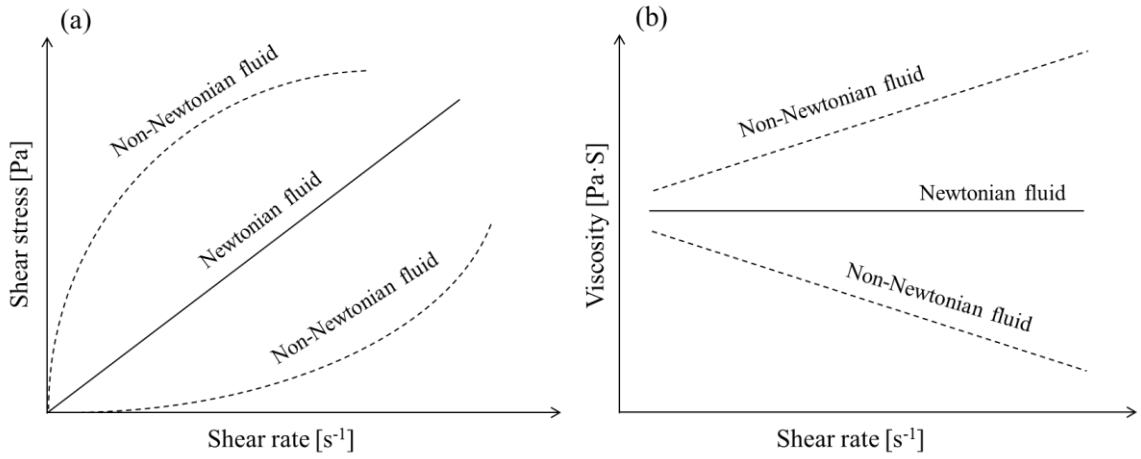

Figure 2.4. Flow curves of Newtonian and non-Newtonian fluids. (a) Correlation between shear rate and stress. (b) The relationship between shear rate and viscosity.

Newtonian fluids are expressed as a constant slope through the relationship between shear rate and shear stress. If the slope is not linear in any Fluids, we can call them non-Newtonian fluids. Non-Newtonian fluids usually are high molecular weight liquids, including solutions of polymers, Polyacrylamide (PAM) and Agar biopolymers (Subramanian, 2014). Bulk viscosity is measured by an acoustic spectroscopy, and is considered the relaxation of both

rotational and vibrational degrees of freedom; whereas, dynamic viscosity is reflected by only rotational molecular motion (Dukhin and Goetz 2009).

Apparent viscosity (η) is the slope of the relationship between shear stress and shear rate. In a shear-thinning fluid, a slope of the relationship between shear rate and the apparent viscosity is decreased with the increase of the shear rate. Most biopolymers are involved in non-Newtonian fluids and have shear-thinning property, shown in Fig 2.5. For example, apparent viscosity (Pa.s) of pullulan and SDS- rich as the liquid is slightly decreased as they increase their shear rate (Spyropoulos et al. 2007). Xanthan solutions have the property of shear-thinning fluid through the reduction of viscosity of increasing shear rate (Comba and Sethi 2009; Amirnia et al. 2013). On the other hand, the tendency of shear-thickening fluid is the opposite. Therefore, the application of biopolymers with shear-thinning properties should be considered, depending on time, location, and the methods of application.

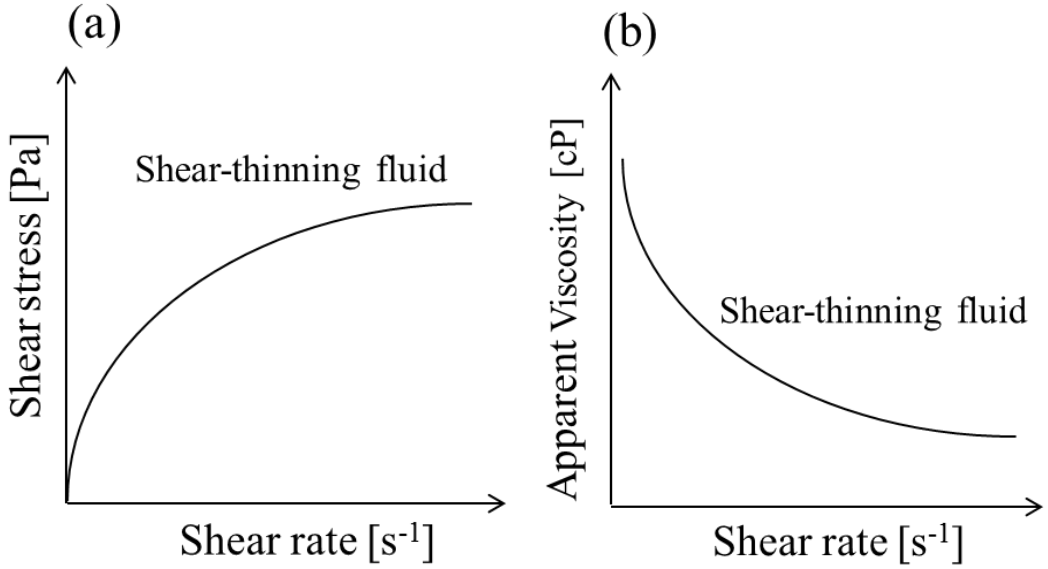

Figure 2.5. Each curve of shear-thinning fluid as a function of shear rate depends on (a) Shear stress. (b) Apparent viscosity.

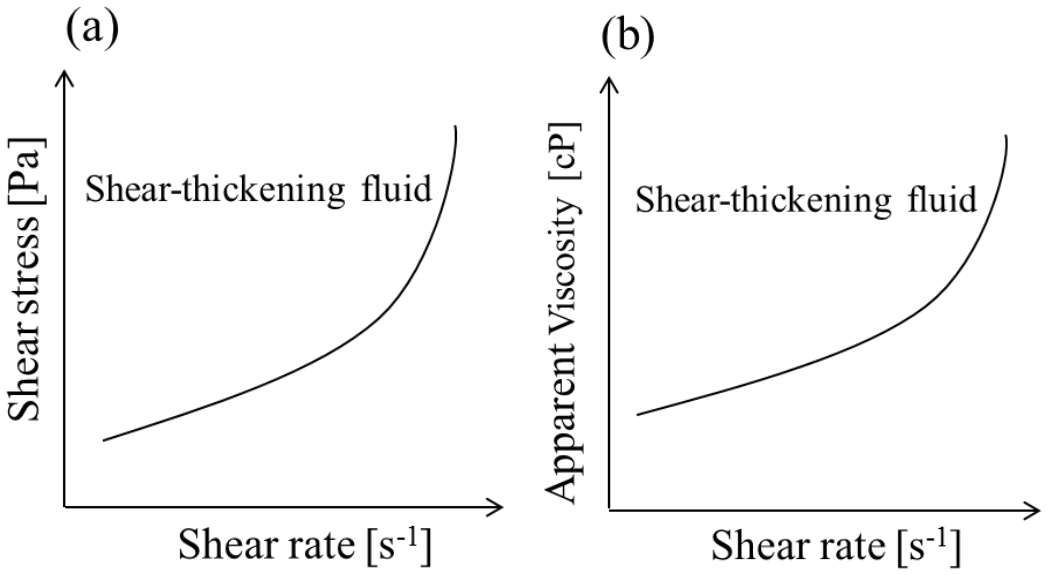

Figure 2.6. Each curve of shear-thickening fluid as a function of shear rate depends on (a) the shear stress and (b) the apparent viscosity.

Viscosity is enormously affected by temperature. Oil samples are measured at different temperatures such as 30, 40, 50, 60, 70, 80, and 90 ℃ (Du et al. 2013). The viscosity of oil samples generally decreases as temperatures increase (Du et. al 2013). However, the influence of oil viscosity of Xia-8, 3950mPa·s, is not significant different from the alkaline flooding efficiency at about 20% at 30℃ and 50℃, but its influence is less than 10% at 70℃ (Du et. al 2013). Therefore, the high viscosity of liquids will obtain higher oil recovery than liquid with low viscosity.

Biopolymers are affected by a shear rate as diverse values. Shear rate ranges from 1 s^{-1} to 104 s^{-1} in order to compare apparent shear viscosity (Pa·s) (Chen 2003). The apparent viscosity of pullulan-rich and SDS-rich is obtained at shear rates of 1 s^{-1} to 102 s^{-1} (Spyropoulos et al. 2007). The apparent viscosity of HAHPAM/silica hybrids is expressed as a function of the shear rate from 1 s^{-1} to 103 s^{-1} (Zhu et al. 2014).

Hydrophobically, associating partially hydrolyzed polyacrylamide, called HAHPAM, is applied when the HAHPAM endures at high-temperatures such as 85 ℃ even though it has shear-thinning property (Zhu et al. 2014). Hydrophobically modified polyacrylamide (HMPAM) is implemented at 65 ℃ as a high-temperature reservoir (Han et al. 2012). To compare biopolymers, Xanthan gum and Guar gum solutions are employed in each different concentration (1.5, 3, and 6 g/L) at 10 ℃, 25℃, and 40℃ (Xue and Sethi 2012).

2.2.3. Contact Angle

The contact angle is defined by the extent of an angle between a liquid drop and solid surface. In geotechnical engineering, a liquid drop is assumed by water and a solid surface is generally considered as soil. The ultimate goal of measuring the contact angle throughout the Young-Laplace equation is to evaluate the wettability of water on the surface of the ground.

We derive the relationship between interfacial tension, capillary pressure, and contact angle using the Young-Laplace Equation in Fig. 2.7 (Weisbrod et al. 2002).

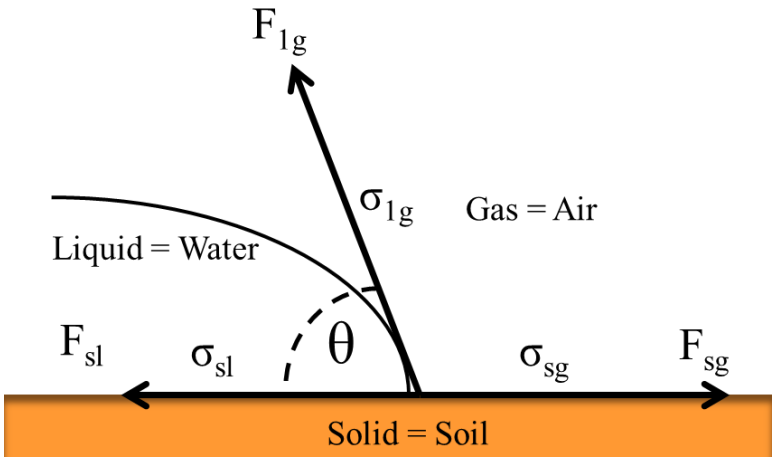

Figure 2.7. Definition of the relationships between interfacial tension, capillary pressure, and contact angle (Weisbrod et al. 2002).

At the center of the three forces, we obtain the equation (2.3) due to their equilibrium;

$$\sum F = F_{sl} - F_{sg} + F_{lg}\cos\theta \quad (2.3)$$

Equation (2.3) is possible to change the Young's equation, especially the surface tension or surface force (Weisbrod et al. 2002; Joanny and Gennes 1984):

$$\sigma_{sg} = \sigma_{sl} + \sigma_{lg}\cos\theta \quad (2.4)$$

where σ_{sg} = the solid-gas interfacial tension

σ_{sl} = the solid-liquid interfacial tension

σ_{lg} = the liquid-gas interfacial tension

θ = the contact angle or Young's contact angle (Yuan and Lee 2013).

The contact angle (γ) of Equation (2.4) plays a paramount role in the Young-Laplace equation. As we know, the Young-Laplace equation (2.5) is the original version, the capillary pressure, *Pc*,

$$\boldsymbol{P_c = \frac{2\sigma lg\cos\theta}{r}} \quad (2.5)$$

The only difference between equations (2.5) and (2.8) is the expression of interfacial tension, γ and σ.

The assessment of surface wettability or wettability is measured by the contact angle (Ryan and Poduska, 2008). It is a very efficient procedure to prove that measuring contact angle shows the effects of roughness and wetting fragment quickly (Ryan and Poduska 2008). Through the measurement of contact angle, when the contact angle of liquid is less than 90 degrees it is termed hydrophilic, while it is defined hydrophobic when the angle is greater than 90 degrees. That is, hydrophilic has high wettability, whereas hydrophobic has low wettability (Yuan and Lee 2013).

The contact angle is influenced by various factors: surface roughness, certain atoms in liquid, and wettability at the interface of liquid-solid-gas (Ryand and Poduska 2008; Yuan and Lee 2013). In addition, the pressure during specific tests may affect results of contact angle due to the possible alteration of the viscosity of a particular liquid (Kim and Santamarina 2014). In order to obtain reliable data, we should measure contact angles using consistent variations.

One of the most popular measurements of contact angle is a sessile drop test, but is not useful due to its error of approximately ± 2° for undersized angles and uneven contact lines (Dimitrov et al. 1991).

2.2.4. Surface Tension

Surface tension is one of the specific properties which characterizes biopolymers. Interfacial tension, very similar to surface tension, refers to the formed interfaces between air/liquid/solids. For example, the value of interfacial tension between a Hexadecane-water is 54.70 ± 3.62 dyne/cm (Jang et al. 2004).

Surface tension is defined as the characteristic of the force when a surface of liquid tries to reduce its area as small as possible. The measurement of surface tension is one of the most difficult tests because it is an irregular value and depends on temperature and pressure, especially the surface tension of liquid. For example, even though the surface tension of distilled water is measured, we obtain different values such as 72mN/m or 72.8mN/m (Rahman et al. 2010; Weisbrod et al. 2002). In addition, another surface tension of distilled water is measured as 73.05 (±0.05) using the Du Nouy ring method (Lee et al. 2012). For this reason, to obtain an accurate measurement, we should carefully consider pressure and temperature (Abdelrahim and Rao

2014). Many researchers prefer to employ the Du Nouy ring method and the drop weight method due to their cost-efficient and straightforward procedures (Lee et al. 2012).

2.3. Soil-Water Characteristic Curve (SWCC)

In geotechnical engineering, the coefficient of permeability and shear strength of unsaturated soil can be predicted by SWCC, with regards to the soil suction (Fredlund 1995). A better understanding of such soil parameters is possible to apply to the field of geotechnical engineering. Also, an estimation of the shear strength of the unsaturated soil may give a stable design of slope, foundations, and Earth retaining structures. Therefore, a better understanding of SWCC is one of the most important things for interpreting unsaturated soil conditions.

The measurements of SWCC are diverse methods and procedures, depending on what expecting results are (Fredlund et al. 2012). Pressure plate cell is applied by matric suctions with a high-air-entry disk. Tempe cell and volumetric pressure plate extractor are also applied by them. Wille geotechnik, Barcelona, and Fredlund pressure plate cell can measure SWCC (Fredlund et al. 2012).

Air-Entry Value (AEV) is the most important factor at a SWCC plot. AEV can estimate the lowest pressure to clean a contaminated liquid between the voids of soil. Researchers and engineers in the field of geotechnical engineering have precisely perceived how two parameters, SWCC and Air-Entry Value, are applied for injecting contaminated liquid, especially water. After obtaining the AEV at certain soils, we can determine the exact pressure to clean it. Over the past decades, chemical grouts have been used by various chemicals, but they are toxic and have side effects in nature. To solve this problem, many researchers in geotechnical engineering recommend the use of biopolymers due to their environment-friendly.

2.3.1. Capillary Pressure: Drain – Imbibition Curve

Capillary pressure, one of the most important concepts to understand in unsaturated soils, is defined as the difference of pressure between two immiscible fluids in both the wetting and non-wetting phases (Moseley and Dhir 1996).

This relation equation is performed as

$$\boldsymbol{P_c = P_{nw} - P_w} \tag{2.6}$$

where Pc = capillary pressure

P_w, P_{nw} = the wetting and non-wetting phases.

Capillary pressure (Pc) is generally called the matric suction (Fredlund and Xing 1994). Eqn (2.1) is rewritten by the terminology of geotechnical engineering:

$$\boldsymbol{P_c = U_a - U_w} \tag{2.7}$$

where Ua = the pore-air pressure

Uw = the pore-water pressure.

Capillary pressure (Pc) is defined by the Young-Laplace equation as well (Lenormand et al. 1988; Revees and Celia 1996; Washburn 1921):

$$\boldsymbol{P_c = \frac{2\gamma\cos\theta}{r}} \tag{2.8}$$

where θ is the contact angle, γ, the liquid-gas interfacial tension, r, the average pore radius. In this study, this equation means that biopolymers' solutions can inject into the pores of soil when their pressure is greater than the capillary pressure (Pc) (Lenormand et al. 1988).

Comprehension of the differences between saturated and unsaturated soil is the highest priority for a better understanding of the Soil-Water Characteristic Curve (SWCC). This concept

is one of the most important for understanding the status of current soils. Both saturated and unsaturated soils contain three main phases in soil mechanics: soil, water, and air. In saturated soil, the two phases consist of only soil and water due to the assumption that the water content of a soil is 100% (Lambe and Whitman 1969). On the other hand, components of three-phases in the unsaturated soil are soil, water, and air due to the assumption that the soil is partially saturated (Das 2005). In addition, the fourth phase is called the "contractile skin," the interface between air and water (Fredlund and Morgenstern 1977). Despite only air as a gas is considered, it should be given different states in unsaturated soils.

SWCC defines the relationship between volumetric water content (θ) and matric suction (ψ) (Fredlund and Xing, 1994). SWCC is an extremely relevant factor to understand the unsaturated soil mechanics (Satyanaga et al. 2013). In addition, the relationship between water content and suction is performed by the soil-water characteristic curve, SWCC, for soils (Fredlund and Xing 1994). SWCC is measured by various apparatuses, such as Tempe cells (Sakaki and Illangasekare 2007). In this study, we measure SWCC using our own apparatus after calibrating it.

Air-entry value (AEV) of soil performs soil suction when air comes into the soil (Fredlund and Xing 1994). Total suction is when the water content of the soil is zero, is less than 1,000,000kPa. Therefore, the maximum soil suction shows from 0 to 1,000,000kPa.
One of the most unusual properties in the SWCC is hysteresis behavior, which means many differences between desorption (drain) and adsorption (imbibition) curves are shown in Fig 2.7. Typical SWCCs are shown in Fig 2.8.

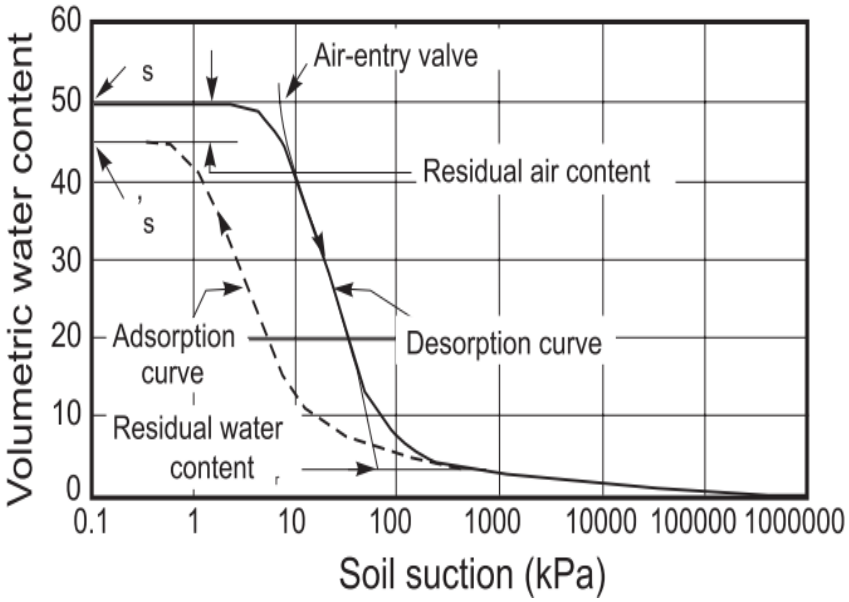

Figure 2.8. Typical soil-water characteristic curves for silt soil (Fredlund and Xing 1994).

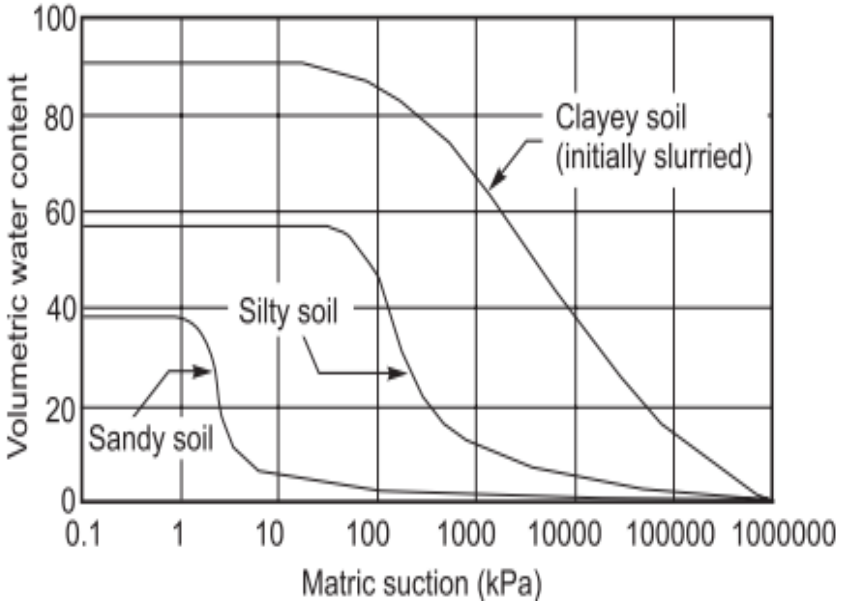

Figure 2.9. Typical soil-water characteristic curves for sandy soil, silt soil, and clayey soil (Fredlund and Rahardjo 1993).

To achieve a better understanding of the physical phenomenon of how the negative pore-water pressure increases the effective stress in the unsaturated soil, it is critical to understand

capillary pressure. Using capillary tubes to describe the phenomenon in unsaturated soil is a useful tool since the surface tension due to air-water-soil interface results in negative pore-water pressure, which leads to the redistribution of water in a capillary tube or unsaturated soil.

The Air-Entry Value (AEV) and residual moisture content, also known as water entry value are the most important parameters to understand SWCC (Satyanaga et al. 2013). AEV is defined as the matric suction when the air first invades between the pores of soil (Satyanaga et al. 2013; Thu 2007). In this study, the 0.5-bar ceramic stone is used as a porous media. To pull out saturated water from the ceramic stone, trapped water in the 0.5-bar ceramic stone needed a pressure of approximate 510cm H_2O to come out the volume of water because 1-bar as a pressure unit equals about 100kPa, 1,020cm H_2O (Lu and Likos 2004).

CHAPTER 3. EXPERIMENTAL PROCEDURES

3.1. Materials

Selecting the biopolymers which are used in this study is one of the most important procedures so that they can be applied for EOR techniques. Numerous researchers recommend Agar and Polyacrylamide (PAM) due to potential availability and many case studies. We select Agar from Alfa Aesar and Polyacrylamide (PAM) from Acros organics in this study.

Ottawa sand F-75 is applied to this study. Soil particles are generally irregular; therefore, they are mixed with all particles great and small. In order to analyze properties of soil particles, we carry out a sieve analysis which results show the particle size distribution of the sand. The results of the sieve analysis are very relevant to permeability and capillarity of the soil (Lambe and Whitman 1969). Figure 3.1 illustrates the results of the sieve analysis of Ottawa sand F-75. More than 95% of the sand is distributed between 0.2mm to 0.5mm (Lu et al. 2009). The average particle size of the sand also is 199μm. Table 3.1 also shows basic soil parameters of the soil.

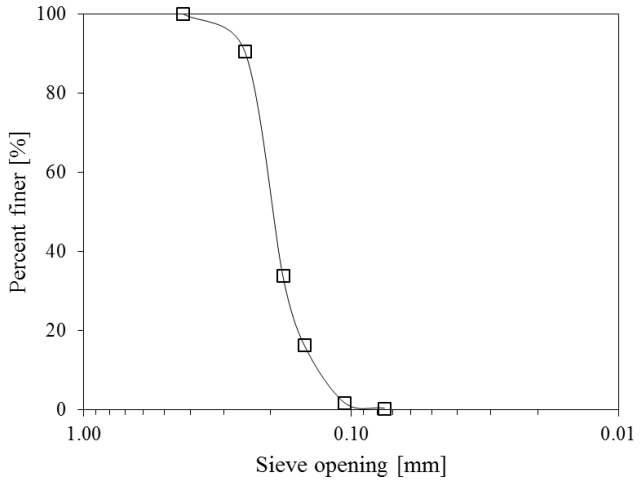

Figure 3.1. Particle-size distribution curves of Ottawa F-75 sand for sieve analysis.

Table 3.1. The basic soil parameters of Ottawa sand F-75.

Ottawa sand F-75	
Average particle size	0.199μm
Effective size, D_{10}	0.140mm
Uniformity coefficient, *Cu*	1.464
Coefficient of gradation, *Cc*	1.007

3.2. Viscosity

In order to measure the viscosity of Agar and PAM solutions, a rotational method is applied with Brookfield Viscometer DV-III (cone) shown in Fig 3.2. The viscosity of Agar and PAM solutions is measured by the resistant force of the geometry to rotating the strength of the motor. As the resistant force is gradually increasing, the viscosity of biopolymers is also rising. The measurement of viscosity discovered by this mechanism.

Both rheometer and viscometer consist of two main parts: A rheometer head (drive motor) and geometry (a spindle) is shown in Fig 3.2. The motor, located at the top spins the geometry at a constant speed.

We measure the viscosity of Agar and PAM solutions with the test plans shown in Table 3.2. The viscosity of every PAM solution with different concentrations is measured by viscometers, but one of the 0.2g/L Agar solutions is measured by the Brookfield Viscometer DV-III since the lowest concentration of Agar solution cannot be measured by viscometers due to the Agar solutions being a gel.

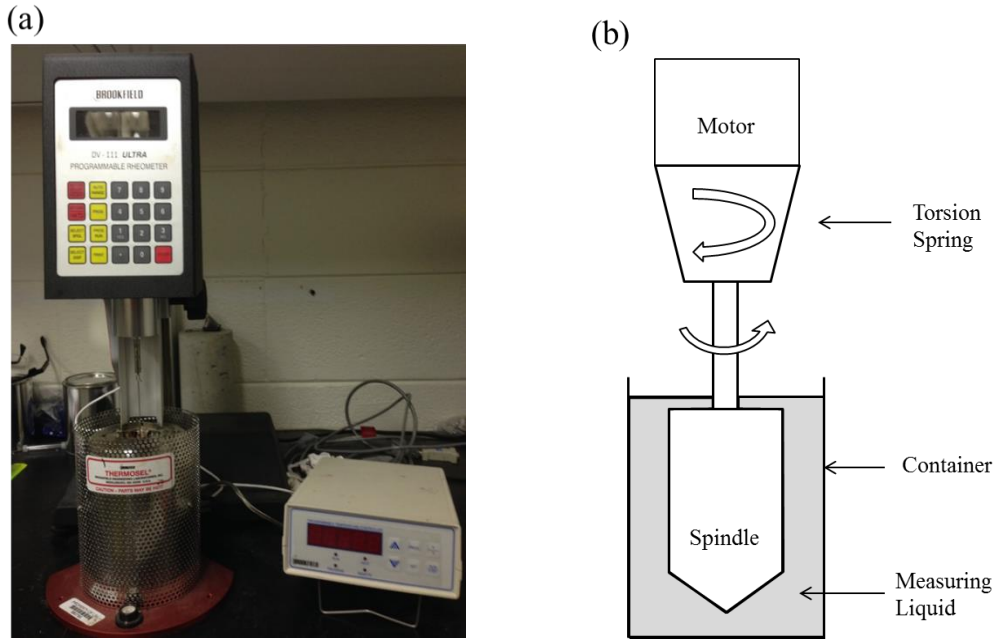

Figure 3.2. Brookfield viscometer model DV-III. (a) A picture in the lab. (b) A schematic design.

Table 3.2. Test plans of the viscosity of Agar and PAM solutions with different concentrations and temperatures using Brookfield viscometer (DV-III).

Brookfield Viscometer DV- III	
Test plans	Agar 0.2g/L at 25, 50, 70, 90 ° C PAM 2,5,10,15,20g/L at 25, 50, 70, 90° C

The procedure of viscosity measurement using the Brookfield Viscometer DV-III shown in Fig 3.2 is very simple and easy. The viscometer consists of two major sections: A rheometer head (motor) and a container. First, the viscometer should be cleaned. The viscometer is leveled on the surface and then it is connected with temperature monitoring. When the rotation of the spindle becomes steady, the running torque is caused by the viscosity and then the twist of the spring is balanced. The twist angle of the spring is proportional to the viscosity of a sample,

which means the extent of viscosity is displayed on the scale. Therefore, we attain the viscosity of the samples.

3.3. Contact Angle

In order to obtain a better understanding of capillary pressure, we conduct a sessile drop method, one of the most popular techniques for measuring contact angles. We prepare a digital camera, glass, syringe, distilled water, and biopolymers' solution for a test of contact angle. Figure 3.3 illustrates performative and calculating contact angles using the ImageJ software by the NIH images. Contact angles are measured at least 5 times in 22 sets: distilled water, 2, 5, 10, 15, 20g/L of each Agar and PAM in the air and in the hexadecane. The least dispersed the of three contact angles among the measured contact angles are performative contact angles.

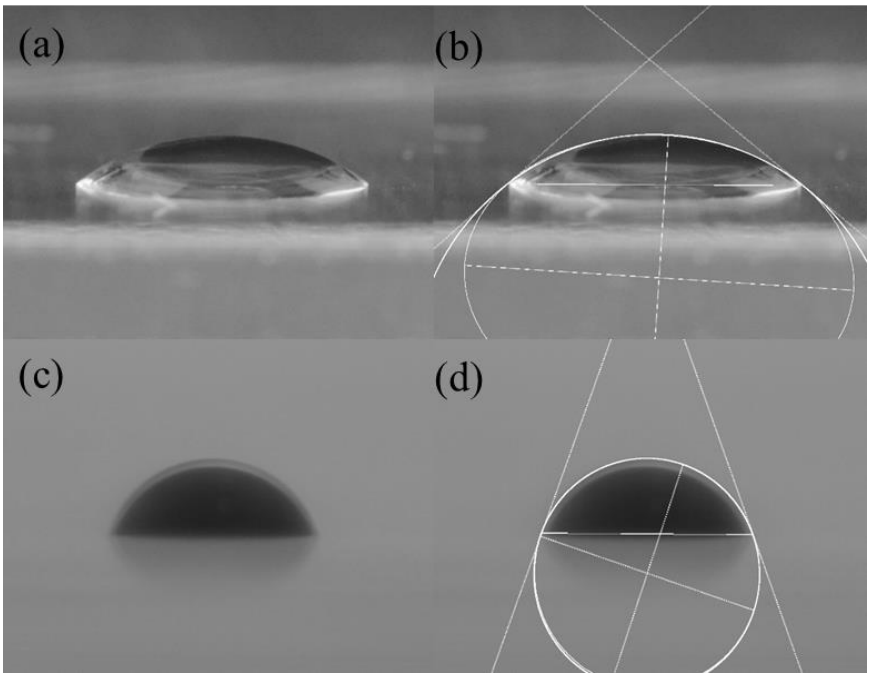

Figure 3.3. The representative images of contact angle with a SiO_2 surface. (a) - (b) contact angles in the air. (c) - (d) contact angles in Hexadecane. (b) and (d) are shown by measuring the contact angle using ImageJ 1.48 software.

Each contact angle test is conducted at the room temperature (25 ℃). After the Agar and PAM solutions are prepared, they are dropped more than 3 droplets to reach at least 3cm height on the glass (mostly SiO_2) assuming soil, without waving of the syringe. We can take accurate pictures after droplets of distilled water, and biopolymer solutions are focused on by a digital camera, as well as, the shapes of droplets which make an ellipse to find interacting points. Therefore, we can take a picture of the droplets as distinct as possible, and then measure the contact angle of biopolymer solutions.

3.4. Surface Tension

The measurement of Agar and PAM solutions is measured by the Du Nouy ring method, one of the simplest methods to test a surface tension shown in Fig 3.4. All biopolymer samples are measured by the Sigma 703D force tensiometer shown in Fig 3.4 We measure the surface tension of PAM solutions (2, 5, 10, 15, 20g/L) and Agar 0.2g/L, 10% of the lowest concentration of Agar solutions is a performative. The measurement of their surface tension is conducted at least 5 times to reduce testing error.

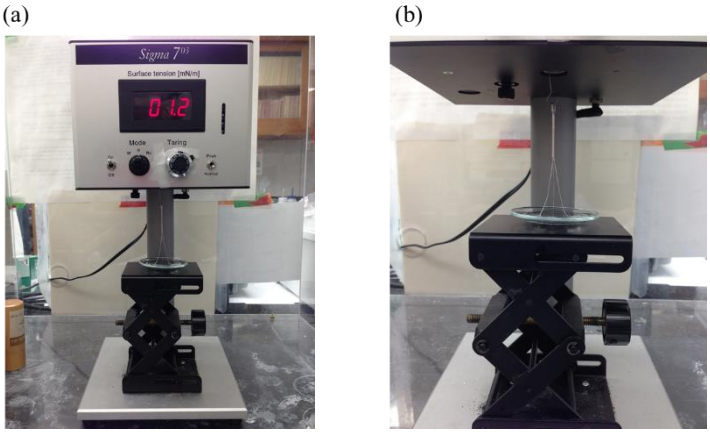

Figure 3.4. Measurement of the surface tension of biopolymers using Sigma 703D force tensiometer. (a) Setup for a test. (b) During the test.

The procedure for measuring the surface tension of biopolymers with the Sigma 703D using the Du Nouy ring method is very simple and quick. A digital display for the value of surface tension is on the Sigma 703D (mN/m) and a lab jack for a sample as well as a 6cm platinum-iridium ring. First, we calibrate the Sigma 703D, measuring range from 1mN/m to 1,000mN/m, to conduct the surface tension test. After the calibration of the Sigma 703D, it turns a switch located on the digital display to R (uncorrected) or RC (corrected) of a label "Mode". A sample solution is put onto the lab jack, and then the 6cm ring is installed on the hook. The knob labeled "Peak/Normal" is placed in the Normal position. The knob labeled "Taring" is turned until the number on the display is zero.

We lift the lab jack with the sample until the 6cm ring is submerged into the sample. After that, we switch the "Peak/Normal" knob to the Peak position. The platform of the lab jack keeps lowering the sample until the sample is separated from the ring's border. At that time, we have to read the maximum value of the sample as a unit of mN/m. The value is the surface tension of the sample. Moreover, for the following test, the Peak/Normal knob switch should be transferred to the Normal position, and then we can measure another sample.

3.5. Microfluidic Models

The microfluidic models are used to verify the sweep efficiency of the Agar and PAM solutions compared to distilled water. However, in this study, only PAM solutions are tested due to the high viscosity of Agar solutions. We inject the PAM solutions into a microfluidic chip, shown in Fig 3.5, with the flow direction, saturated in the n-hexadecane which acts as an oil reservoir to measure the displacement ratio (Pore saturation) of the PAM solutions. Obtained results are analyzed to find the sweep efficiency of the PAM solutions.

The microfluidic chip (20 x 10mm) used in microfluidic models are made of silicon dioxide, also known as SiO2, which assumes the role of natural soil due to the high similarity between them. Its pore spacing and depth are 30μm and 60μm, respectively. Pores and pore throats are formed by 600 circular micro-particles, which are 700μm in diameter. The total number of pores used to evaluate the displacement ratio is 1085. As they are saturated with PAM solutions, we observe the pattern of fluid flow as well as the displacement ratio by injecting PAM solutions through 2-D network models during the test.

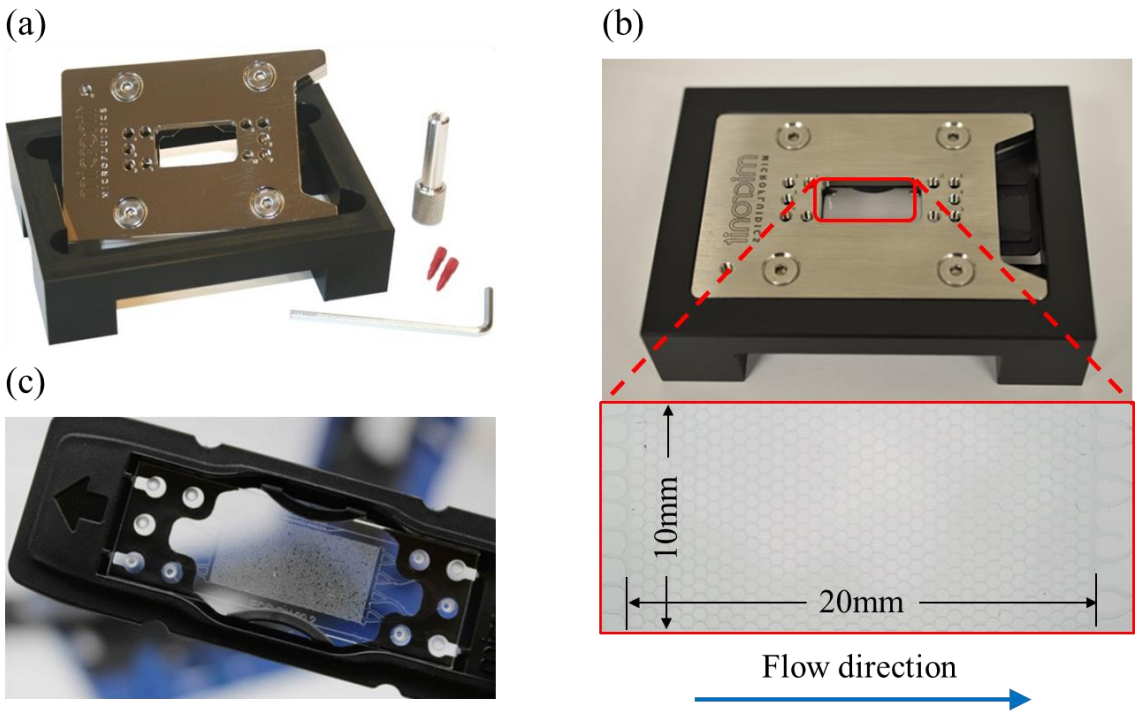

Figure 3.5. The components of the microfluidic models. (a) Chipholder kit. (b) A setup of chip holder and an enlarged microfluidic chip. (c) The microfluidic chip.

Fig 3.6 illustrates the setup of the microfluidic models and a schematic design. We prepare a digital camera, a syringe pump, the ISCO pump, and microfluidic models. The digital camera is used to take pictures when the biopolymer solutions saturate the microfluidic chip. The syringe

pump can control flow rates of the biopolymer solutions to analyze how much the flow rate influences the results of displacement efficiency. To clean the microfluidic chip, over 2,000kPa CO_2 from the ISCO pump is used after each test finishes to minimize potential errors.

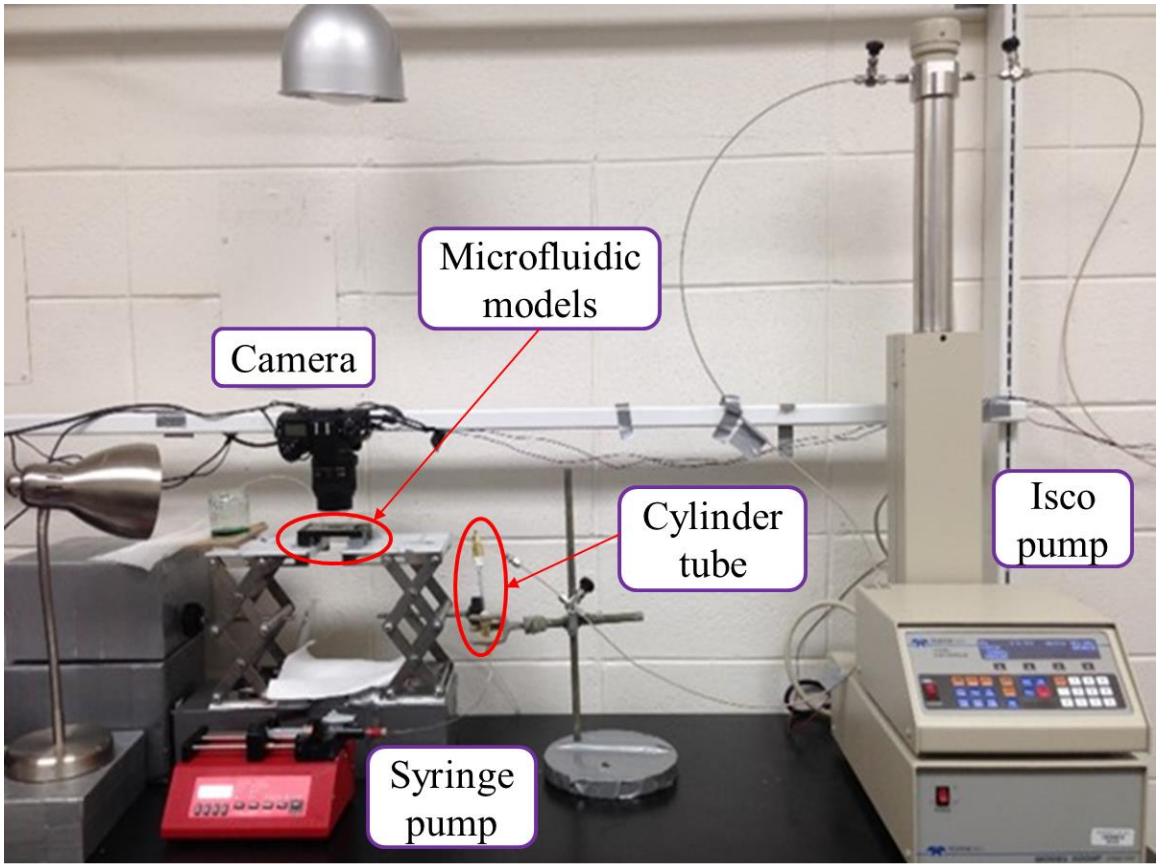

Figure 3.6. The experimental setup for microfluidic models.

The two main procedures of the microfluidic models are composed of testing, flushing, and cleaning, shown in Fig 3.6. Due to micro-scale particles of the microfluidic chip, a flushing process is imperative. In Fig 3.7 (a), all straight lines are connected by tubing from syringe pump to waste during testing. In 3.7 (b), both the microfluidic chip and the ISCO Pump directly are connected. At this time, a tubing, located at the top of cylinder tube, is disconnected, shown in Fig 3.7 (b) during flushing and cleaning. After we finish a single test using microfluidic models,

we have to flush and clean every tubing because residual biopolymer solutions inside tubing can affect the concentration of a measuring biopolymer solution. The procedures of flushing and cleaning are one of the most important things in the microfluidic models.

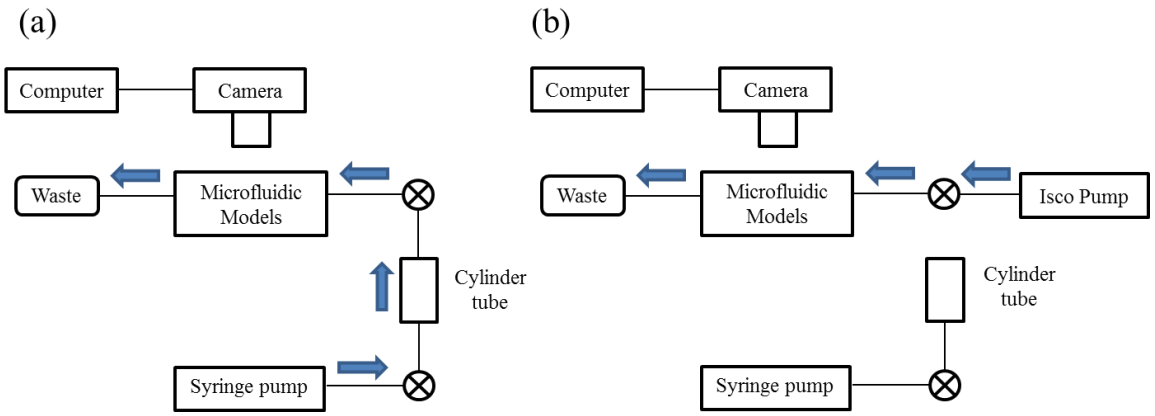

Figure 3.7. The schematic designs of the experimental setup for Microfluidic models. (a) Testing. (b) Flushing and cleaning.

The microfluidic models are conducted using the following liquid: Distilled water, Agar and PAM solutions (Concentration: 2, 5, 10, 15, 20g/L, flow rates: 0.3µl/min, 1µl/min, and 5µl/min). The microfluidic models also are conducted using two distinct conditions: in the air and the Hexadecane, which assumes the role of an oil reservoir.

First, procedures of injecting biopolymers in the air are explained for microfluidic models in sequence. The microfluidic chip is located at the center of focus of a digital camera to take high-quality pictures. The chip should be entirely cleared by injecting alcohol and CO_2 until saturated to eliminate any contaminants. The chip is naturally dried at room temperature until perfectly dried. In Fig 3.7 (b), injecting CO_2 from the ISCO pump cleans the chip through the connected fitting tube to the chip. After cleaning inside the chip, alcohol is injected using a

syringe to eliminate minute potential residuals of the biopolymer solutions. By using a digital camera, we can verify the cleanness of the chip.

In the air, distilled water and solutions of Agar and PAM for microfluidic model tests are easily measured. Measuring solutions are injected into the microfluidic chip; they start from a syringe. First, we check the clearness of the microfluidic chip. Each solution is injected by using the syringe pump device as individual constant flow rates are controlled. Distilled water, Agar and PAM solutions (2, 5, 10, 15, 20g/L) are tested by individual flow rates (0.3µl/min, 1µl/min, and 5µl/min). After the chip is entirely saturated, they keep injecting to find the convergence of the particular value of saturation as each solution is injected over 100 times. While injecting solutions, we take proper pictures or record a video with a DSLR camera. Therefore, the microfluidic model tests are repeated to obtain reliable results and then collected data is carefully analyzed.

The procedures of another method of the microfluidic models in the hexadecane assumed as an oil reservoir are slightly different than the former ones. The procedures are the same until the chip is flushed and cleaned. First, injecting hexadecane is to saturate a microfluidic chip. The pores of microfluidic chip assumes the role of and oil reservoir. A fitting tube between the top of the cylinder tube and the microfluidic chip have to be filled by hexadecane to prevent flowing air to oil-water or oil-biopolymer solutions interfaces. After the fitting tube is disconnected, shown in Fig 3.7 (b), biopolymer solutions using the syringe pump are injected into the cylinder tube until they reach the top of the cylinder tube and form semi-circular droplets. The fitting tube reconnects to the top of the cylinder tube without flowing air. If air comes between the oil-liquid

interfaces, the setup has to reset to eliminate fatal errors. Each step is carefully set to obtain accurate results.

After verification of no leakage and the inflow of air, we collect the results of the microfluidic model tests. Distilled water and Agar/PAM solutions with absolute constant flow rates are injected into the microfluidic chip until a fitting tube in the outlet direction is saturated by them. During the test, we take at least 5 pictures or record the pattern of displacement ratio to analyze how Agar/PAM solutions are more efficient than distilled water.

We have to clean and flush the microfluidic chip as well as every tubing after every procedure is done because biopolymer solutions may be hardened by chemical reaction. As following the steps, Table 3.3 illustrates the microfluidic model tests which are conducted.

Table 3.3. The implements of distilled water and Agar/PAM solutions in the air/hexadecane for Microfluidic models.

Type	In the air	In the Hexadecane
Distilled Water	O	O
*Agar + Distilled Water	O	
† PAM + Distilled Water	O	O

*A status of Agar added distilled water to a mixture.

† PAM solutions with distilled water are perfectly blended with a liquid.

3.6. Soil-Water Characteristic Curve (SWCC)

To obtain an SWCC, we carry out its test in the lab by manufacturing devices shown in Fig 3.8 and 3.9. These devices consist of two main sections: a chamber and a measuring tube. After bottom of each chamber, each 0.5-bar ceramic stone (Diameter = 8.026cm and thickness =

1.067cm) in Table 3.4 as a porous media is set up. Afterward, flexible PVC tubing connects with a 3-way valve that control the flow of water to overcome its insufficient lengths for measuring total volumes of water in the voids of soil. The measuring tube is also connected to the 3-way valve to calculate the quantity of water that comes out from a soil with a particular capillary pressure (Pc). First, the camber have to be calibrated using distilled water. Once the apparatus works well, sand is filled into the chamber. The height of water into the chamber is the same with the measuring tube. Therefore, this means that we are ready to start the SWCC test. The properties are summarized with 0.5-bar ceramic stones as porous media, which are used for the SWCC test in Table 3.4.

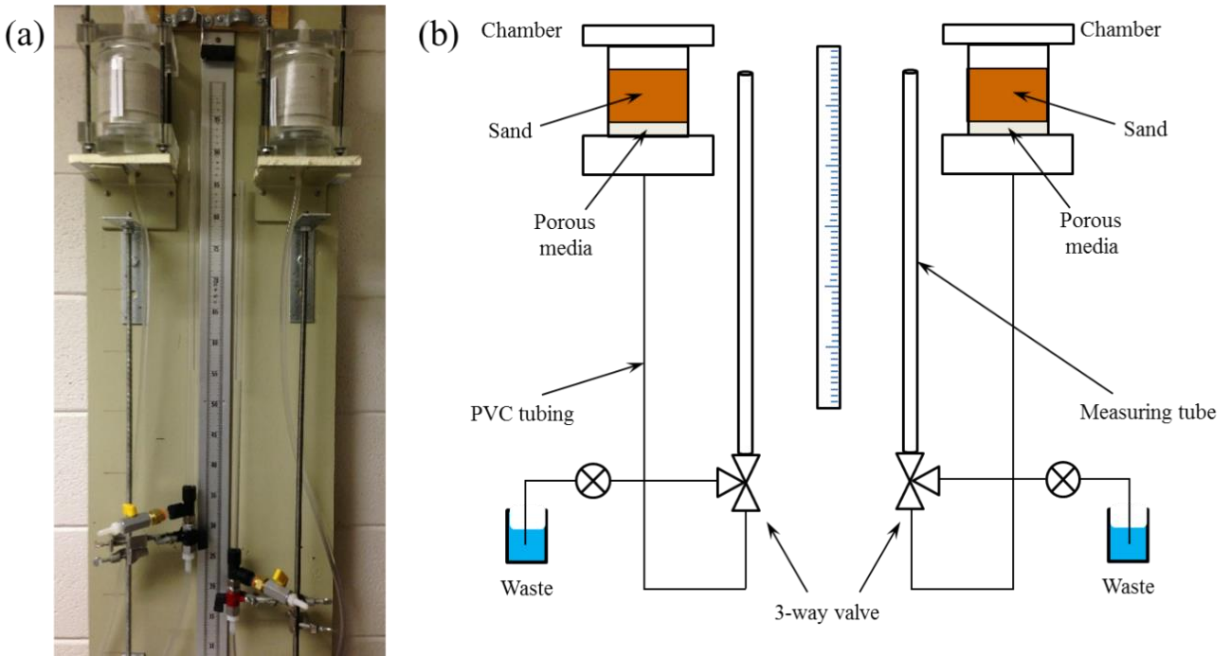

Figure 3.8. The setup of SWCC tests. (a) In the lab. (b) The schematic design.

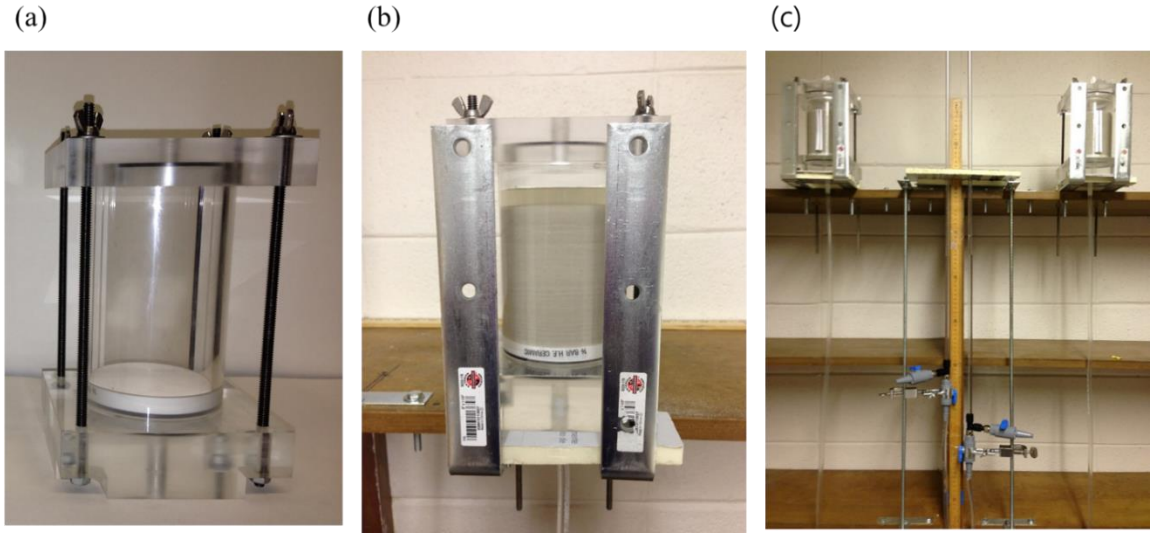

Figure 3.9. The pictures of SWCC tests. (a) A chamber (b) the setting chamber with sand and water (c) the setup of SWCC tests prior to the experiment.

Table 3.4. The properties of Ottawa sand F-75 and 0.5-bar ceramic stone.

	Ottawa sand F-75	0.5-bar ceramic stone
Porosity, n	0.381	≈ 0.500
void ratio, e	0.616	≈ 1.000
Hydraulic conductivity, k, cm/s	4.96×10^{-2}	3.11×10^{-5}
Specific gravity, G_s	2.65	

After we set up the device for obtaining an SWCC, we start to calibrate the flow throughout every flow path such as the chamber, porous media, PVC tubing, and 3-way valves. The properties of the chamber are shown in Table 3.5. Without the soil, water is filled in the entire system. And water levels at the measuring tubing fit the same level at the chamber. After two water level are the same, water level at the measuring tubing is raised more than 10cm. If the water level decreases within 5min without any pressure, water can flow through the porous

media by the difference of capillary pressure. As a similar method, after the water level is decreased compared to the one at the chamber, we wait at least 5min. If the water is raised at the measuring tubing, the device is working well. Otherwise, we check out every single part to ensure it functions well.

Table 3.5. The properties of four chambers for SWCC test

	Chamber #1 & # 2	Chamber #3 & # 4
ID (cm)	8.255	7.620
The height of soil (cm)	7.620	8.915
The volume of soil (cm^3)	406.550	406.573
The weight of soil (g)	666.397	666.436
ID of measuring tube (cm)	0.953	635

Approximately 666g Ottawa sand F-75 is put into the chamber after we make sure the calibration of the device for measuring SWCCs is correct. In order to obtain more accurate data, residual air in the voids of the sand should be removed by using the oven at 95℃ at least 2 hours before the sand is put into the chamber. After that, the the water level above the soil should be the same level with the water level of the chamber to determine the datum. To do this, once the water level at the measuring tubing is laid the point lower than water level in the chamber, the water level at the measuring tubing will be slowly or quickly increased depending on the concentration of PAM solutions because residual water in the soil should come out to equal the water level using Bernoulli's equation (Das 2005). These procedures will take from a few

minutes to hours depending on the concentration of the PAM solutions. When both water levels are the same, we can start to test for drawing an SWCC.

The process of drawing the SWCC is very simple, but time-consuming work. At the first equilibrium level, if the water level at the measuring tubing moves 5cm below the datum, it means 5cm is the current capillary pressure. When the water level is down, water should come out from the soil to equalize the water level. At this time, we can collect the volume of water until the water level never increases at the first planned point. Obtained volume of water means that the total volume of water is decreased. That is, the degree of saturation of water as the initial condition, 100%, will be reduced as much as the water comes out. Through these procedures, we can draw an SWCC as the degree of saturation (%), x-axis, and capillary pressure (cmH_2O), y-axis.

CHAPTER 4. EXPERIMENTAL RESULTS

4.1. Viscosity

The viscosity of biopolymer solutions are measured by the Brookfield viscometer (DV-III): Distilled water, 2 ~ 20g/L PAM solutions, and 0.2g/L Agar solution. The properties of the viscometer are shown in Table 4.1.

Table 4.1. The properties of Brookfield viscometer (DV-III).

Brookfield viscometer (DV-III)	
System	Rotational
Speed Range	0-250 RPM
Temperature Range	-100 ℃ – 300 ℃
Viscosity Accuracy	± 1.0% of full-scale range for a particular spindle running at a specific speed
SPINDLE	SC4 - 27
Shear Rate Constant (SRC)	0.34
Shear Rate (s^{-1})	0 - 68
Viscosity Range (cP)	9.4 – 234.325

The measurement of viscosity is simple and straightforward using the viscometer. However, viscosity is vulnerable to the variation of temperature and usually decreases when the the temperature increases. The maintenance of temperature is the most important factor to measure biopolymer viscosity accurately.

The viscosity of distilled water is 1.005 centipoises (cP) at 20 ℃ using Ostwald viscometer, which can control temperature within ±0.02 deg (Hardy and Cottington 1949).

However, the viscosity of distilled water is irregular, even though it should be the same viscosity regardless of shear rates since it is Newtonian fluid. The primary reason for this irregularity is temperature. Theoretically, the temperature of the viscometer should be constant during the test, but it usually fluctuates due to the effects of air. Therefore, the measured viscosity of distilled water has the same tendencies as Non-Newtonian fluids.

The viscosity of Agar and PAM solutions is measured by the Brookfield viscometer (DV-III). PAM solutions are measured at four different temperature (25, 50, 70, 90℃) and the Agar solution is only measured at 0.2g/L concentration. Even though, the lowest concentration (2g/L) of Agar solution cannot be measured by using the viscometer due to the gelation state of Agar. To solve this problem, we measure at 0.2g/L Agar solution which is formed as a liquid, not 2g/L Agar solution as a gel. In addition, the viscosity of the lowest Agar solution is expected to be greater than the viscosity of the 0.2g/L Agar solution because it is a gel.

The viscosity of the 0.2g/L Agar and every PAM solution shown in Fig 4.1 decreases with an increment of shear rates due to the non-Newtonian behavior of biopolymers. Moreover, as the temperature of the biopolymer solutions increases, their viscosity usually reduces. An increase of the shear rate at the same concentration of solution affects the decline in viscosity.

The viscosity of the 0.2g/L Agar solution is the clearest, rather than the PAM solutions. Even though the 0.2g/L Agar solution is just 10% of the 2g/L Agar solution, its viscosity is higher than the viscosity of the 20g/L PAM solution at room temperature, especially at lower shear rates (up to 20). Through this fact, we estimate that the viscosity of the Agar solution will be higher than one of the PAM solutions at the same concentration. All viscosities of the measured solutions are shown in Fig 4.1.

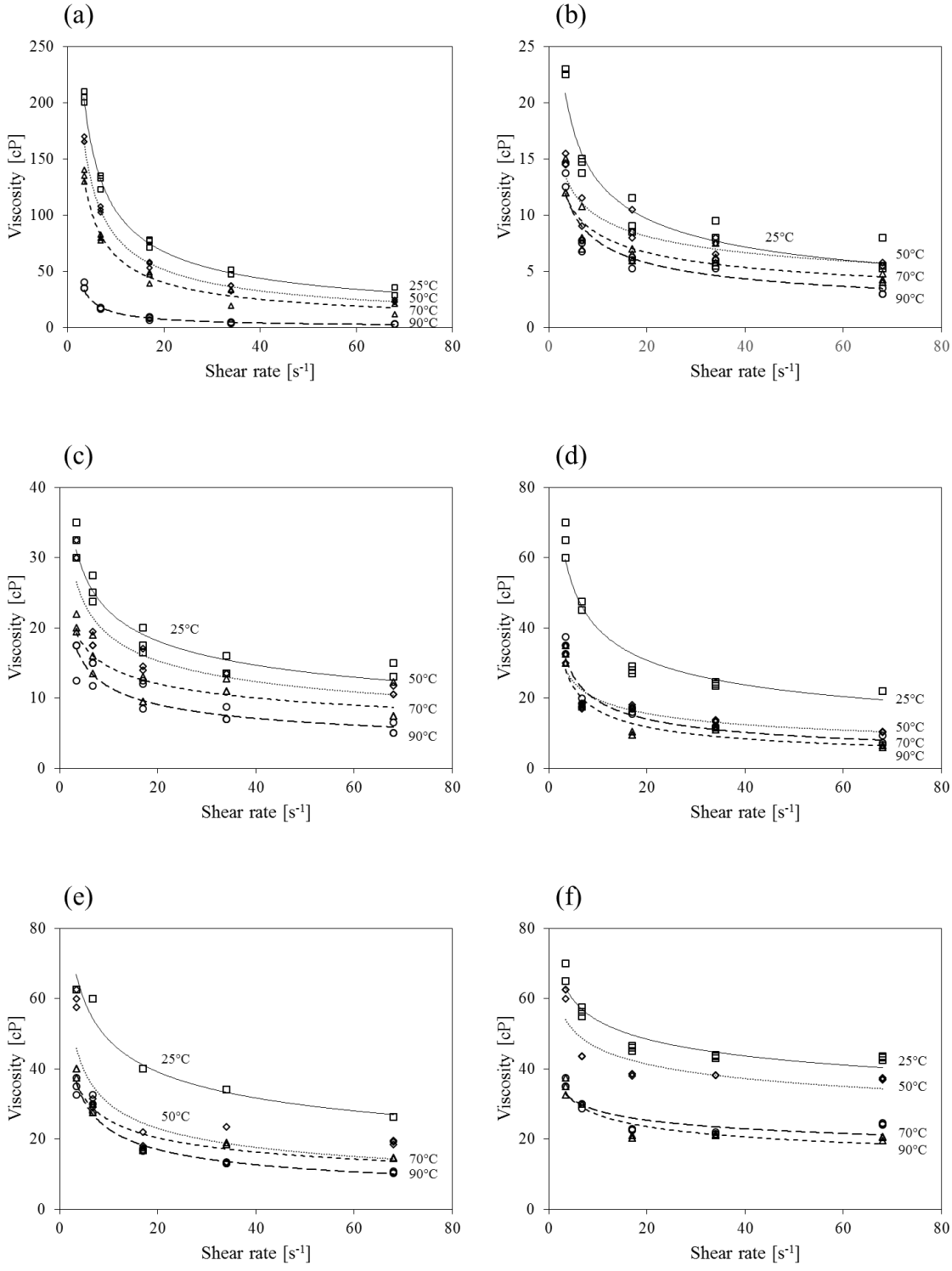

Figure 4.1. Effect of temperature on viscosity: (a) 0.2g/L Agar, (b) 2g/L PAM, (c) 5g/L PAM, (d) 10g/L PAM, (e) 15g/L PAM, (f) 20g/L PAM solutions using the Brookfield viscometer (DV-III).

Each solution has various ranges of viscosity. The range of viscosity of the 0.2g/L Agar solution is from 2.8cP to 210cP. The range of viscosity of the 2g/L and the 5g/L PAM solutions is from 3.0cP to 23cP and from 5cP to 35cP, respectively. Their viscosity is similar due to the minute differences of the concentrations of the solutions. In addition, the boundary of the viscosity of the 10g/L and the 15g/L PAM solutions are from 6cP to 70cP and from 10cP to 62.5cP, respectively. Moreover, the range of viscosity of the 20g/L PAM solution and the 0.2g/L Agar is quite different, even though, the gap between the concentrations of both solutions is separated by a multiple of 10. Therefore, the range of the viscosity is affected by the concentration of the solutions or types of biopolymer solutions.

4.2. Contact Angle

The variations of the concentrations of Agar and PAM solutions in relation to the contact angles in the air and the hexadecane are illustrated in Fig 4.2. All contact angles are measured by the digital camera, and the three obtained contact angles are analyzed by ImageJ 1.48v software using the plugin “contact angle”. They are reliable because the standard deviation of the three contact angles at the same concentration of Agar and PAM solutions is smaller than 1.0, which means three different values are close to each other. In Fig. 4.2 (a), the concentration of both the Agar and PAM solutions in the air increase as their contact angles increase. On the other hand, in the hexadecane, the concentration of Agar solutions increase as their contact angles decrease. Whereas the tendency of the PAM solutions with respect to its concentration is unclear, as shown in Fig 4.2 (b).

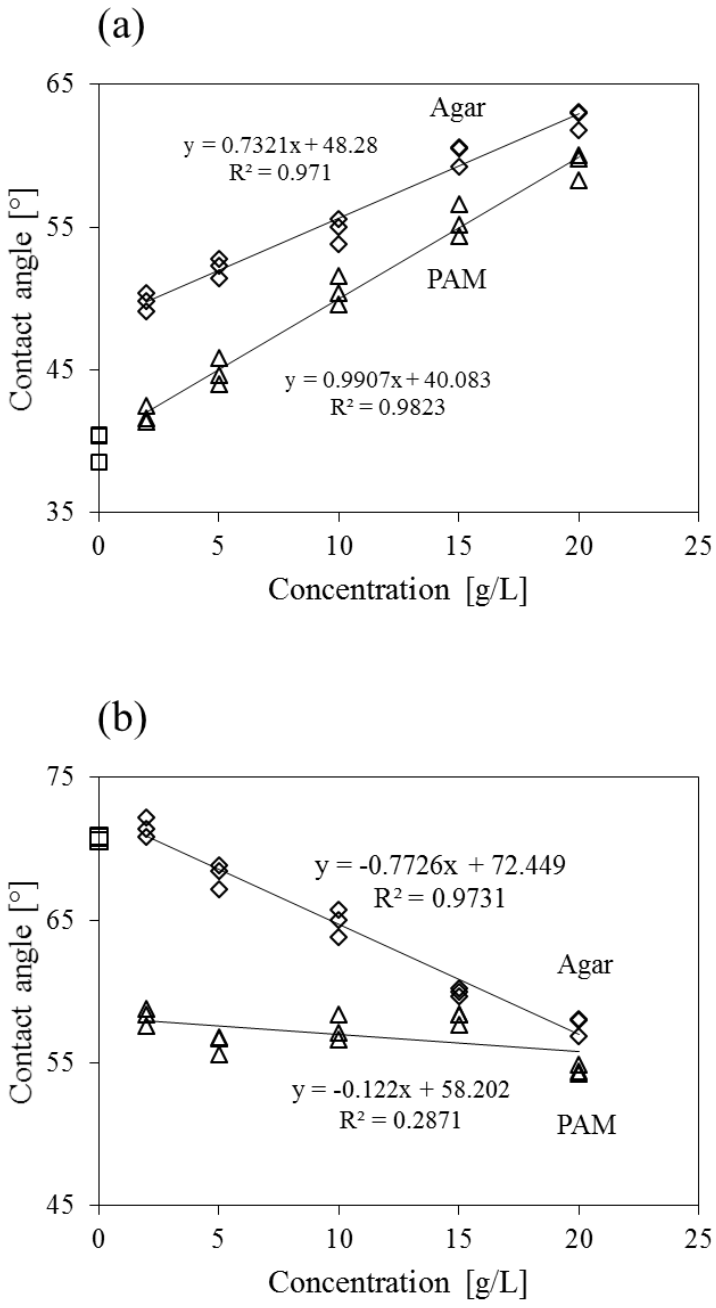

Figure 4.2. The effect of different concentration of Agar and PAM solutions on contact angle, compared with distilled water: (a) In the air. (b) In the hexadecane.

The results of the contact angle tests show that they have a hydrophilic property in the air and the hexadecane because the contact angles of the Agar and PAM solutions are mostly less than 90

degrees. In the microfluidic models, the displacement ratio of the PAM solutions in the Hexadecane gradually increase as a function of flow rate. The displacement ratios, also known as the sweep efficiency, of the PAM solutions, are very efficient at the flow rate of 0.001ml/min when compared to distilled water.

4.3. Surface Tension

The surface tension of the Agar and PAM solutions is measured by the Sigma 703D tensiometer three times. The results of the surface tension tests of the 0.2g/L Agar and PAM solutions (2, 5, 10, 15, 20g.L) at room temperature (25 ℃) are shown in Fig 4.3. The viscosity of distilled water is approximately 72.0mN/m at room temperature (25 ℃) (Vargaftik et al. 1983). The viscosity of the 0.2g/L Agar solution is from 64.9 to 65.1mN/m, and the viscosity of the PAM solutions is from 63.3 to 68.3mN/m. The viscosities of both solutions are generally smaller than distilled water. Therefore, the relationship between the concentration of solutions and surface tension is not relevant.

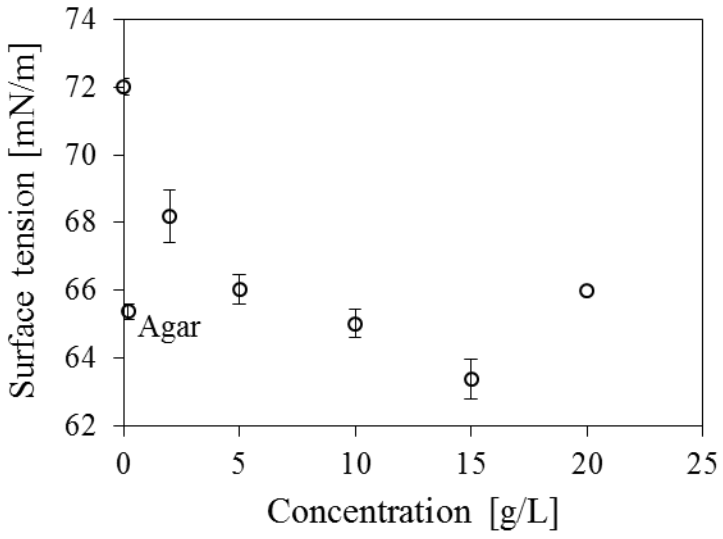

Figure 4.3. Surface tensions of 0.2g/L Agar and PAM solutions at the room temperature (25 ℃).

4.4. Microfluidic Models

The results from the microfluidic models are illustrated in Fig 4.4. The tests are conducted using only PAM solutions (2, 5, 10, 15, 20g/L) and distilled water (0g/L). Each test is conducted with a constant flow rate (0.3, 1, and 50μl/min or 0.0003, 0.001, 0.05ml/min) using a syringe pump at room temperature (25 ℃). Pore saturation of voids in the soil is analyzed by microfluidic models to evaluate the characteristic flow of the PAM solution in voids when it is injected into the ground.

The relationship between the pore saturation (Displacement ratio) and the PAM solutions is relevant. The pore saturation of the PAM solutions at different concentrations (2g/L ~ 20g/L) in the Hexadecane (assumed as an oil reservoir) are always higher than one of distilled water (0g/L PAM) at all flow rates shown in Fig 4.5 (a). At the flow rate of 0.0003ml/min, the pore saturation of the PAM solutions (59.4 ~ 66.6%) are no largely different compared to distilled water (56.9%) in Fig 4.4. However, at the flow rate of 0.001ml/min, the differences of pore saturation between distilled water (58.5%) and PAM solutions (71.4 ~ 98.2%) are enormous. In addition, at the flow rate of 0.05ml/min, pore saturation is very similar to the flow rate of 0.0001ml/min: Distilled water (71.1%) and PAM solutions (88 ~ 99.5%). The higher concentration of the PAM solutions increases the displacement ratio (12.9% ~ 39.6%) at the flow rate of 0.001ml/min and 17% ~28.5% at the flow rate of 0.05ml/min. A Higher concentration of PAM solutions is not relevant to higher displacement ratios in the oil reservoir. In Fig 4.4 (b), the pore saturation of PAM solutions increases with the increment of the flow rate of the PAM solutions.

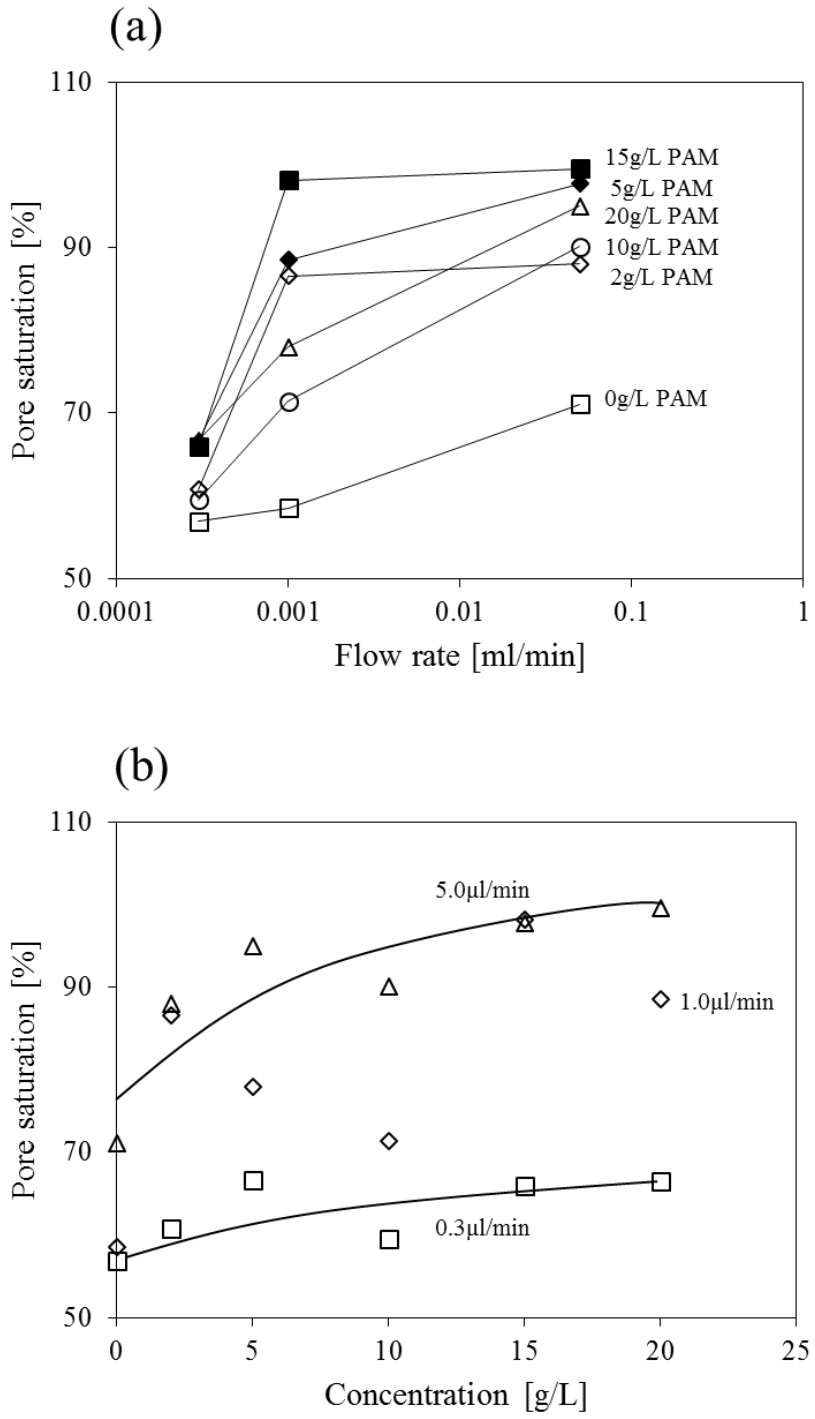

Figure 4.4. The effect of PAM solutions using microfluidic models on pore saturation in the Hexadecane depends on (a) flow rate on a log scale (b) its concentration.

4.5. Soil-Water Characteristic Curve (SWCC)

SWCCs are measured by our own devices. To measure them, we calibrate the device using distilled water through four chambers shown in Fig 4.5. The range of the capillary pressure of H_2O is approximately 32 ~35cm, which means that the standard deviation (0.916) of capillary pressures of the eight values using the four chambers is less than 1.0. Therefore, the chambers are reliable to measure SWCCs of biopolymers.

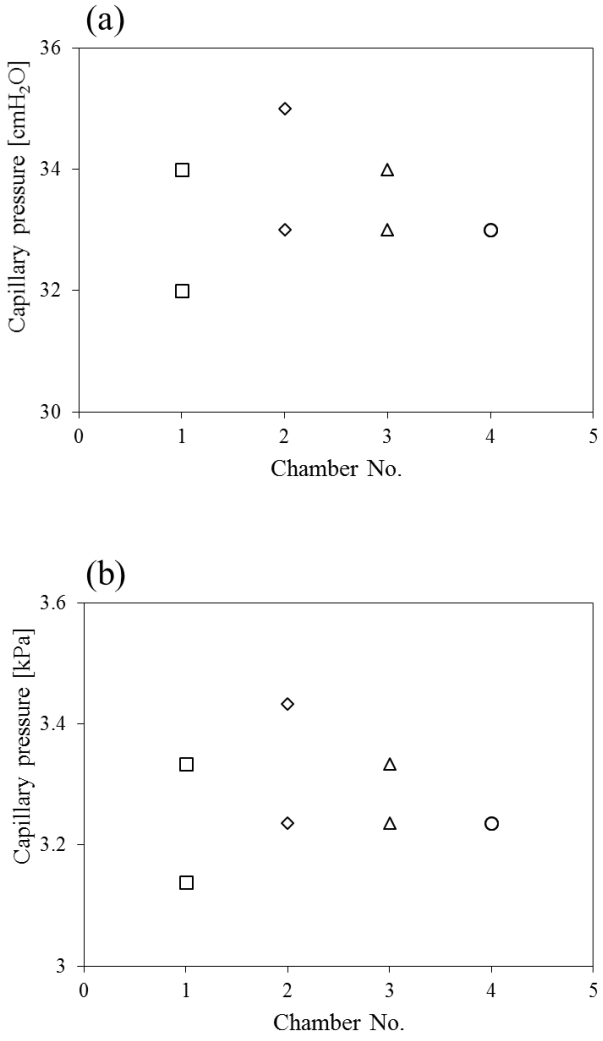

Figure 4.5. The calibration of each chambers using distilled water for capillary pressure (a) as a unit of cmH_2O, (b) kPa.

The performative SWCCs of distilled water using each chamber are shown in Fig 4.6. The relationship between degree of saturation (Sw) and capillary pressure (Pc) is called as Pc-Sw.

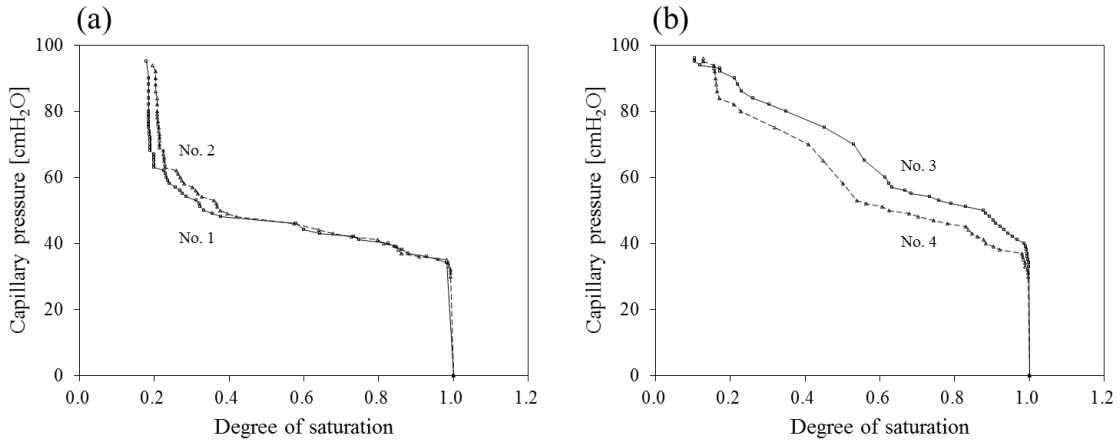

Figure 4.6. The Pc-Sw relationships of distilled water with four chambers: (a) No. 1 and No. 2. (b) No. 3 and No. 4.

The SWCCs of the 2g/L PAM solution are performed in Fig 4.7. The Air-Entry Values (AEV) of two SWCCs are approximate 75 cm. The comparison of capillary pressure between distilled water and the 2g/L PAM solution is approximate 40 ~ 43 cm (about 4kPa).

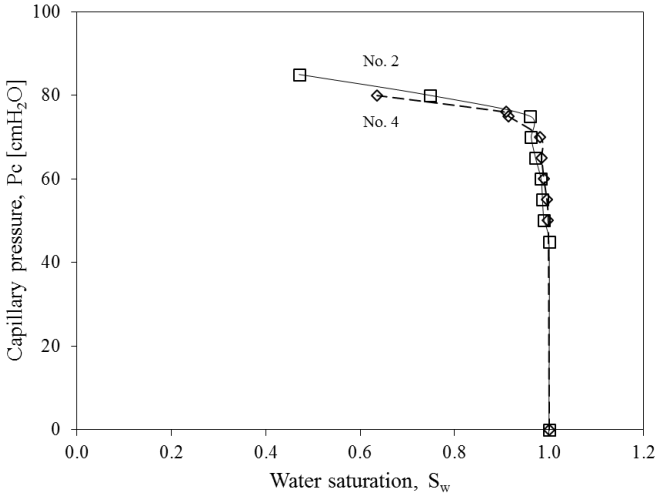

Figure 4.7. Pc-Sw relationships of 2g/L PAM solution with chamber No.2 and No. 4.

CHAPTER 5. ANALYSES AND DISCUSSION

The results of the diverse tests in Chapter 4 are analyzed and discussed in this section. Analyses and discussion are closely related with microfluidic models and SWCC tests. In the microfluidic models, the results of contact angle, viscosity, and surface tension of biopolymers will be applied for analyzing the capillary number (C) and the mobility ratio (M). In the SWCC, we measure a capillary pressure using an instrument manufactured in the laboratory and also calculate it with an equation like a function of effective stress to compare with the results of using the instrument and the equation (Espinoza and Santamarina 2010).

5.1. Analyses and Discussion

The measurement of contact angles verifies two reasonable results. First, contact angles of the Agar and PAM solutions in the air are always greater than the contact angles of distilled water shown in Fig 4.3 (a). However, the Agar and PAM solutions still have a hydrophilic behavior to a glass of silica dioxide (SiO2) because their contact angles are still smaller than 90 degrees in the air. Second, in the hexadecane, increasing concentration of the Agar and PAM solutions generally decreases their contact angles. Due to the hydrophilic properties of every contact angle of the Agar and PAM solutions, they have the same tendencies in the air.

Through the results of viscosity and surface tension tests, we can obtain two parameters with the flow rate of the Agar and PAM solutions: Capillary number (C) and Mobility ratio (M). The capillary number (C) and mobility ratio (M) of the Agar and PAM solutions can be distinguished by three aspects that are stable displacement, viscous fingering and capillary fingering using Fig 2.3 (Lenormand 1990; Sinha and Wang 2007). The capillary number (C) is

obtained by the velocity of the Agar and PAM solutions as a non-wetting phase as well as their surface tension and viscosity. The mobility ratio (M) of the Agar and PAM solutions are derived by the viscosity of the wetting (distilled water and hexadecane), non-wetting (Agar and PAM solutions) phases. These values are achieved from each test in the chapter 4 and analyzed in this chapter.

Figure 5.1 illustrates how the mobility ratio (M) of the Agar solutions (2, 5, 10, 15, 20g/L) and distilled water (0g/L) affects pore saturation at three different flow rates (0.3μl/min, 1.0μl/min, 50μl/min) at room temperature (25°). When the values of Log M increase, the pore saturations of the Agar solutions are always greater than the pore saturation of distilled water, regardless of the velocity of injecting Agar solutions. The smallest difference of pore saturation between 5g/L Agar solutions and distilled water is only 5.1% at the flow rate of 0.3μl/min shown in Fig 5.1 (a). In addition, at the flow rate of 1.0μl/min, the difference of pore saturation is just 5.6% between 20g/L Agar solution and distilled water shown in Fig 5.1 (b). Therefore, the lowest differences of the pore saturation between the Agar solution and distilled water at the flow rate of 0.3μl/min and 1.0μl/min are 5.1% and 5.6%, respectively.

On the other hand, the difference of the least pore saturation between 15g/L Agar solution and distilled water at the flow rate of 50μl/min is 10.5% shown in Fig 5.1 (c) and (d). This difference is about twice, compared with the flow rate 0.3μl/min and 1.0μl/min. That is, this means that the pore saturation of the faster flow rate of Agar solutions can be rarely affected, rather than the slower flow rate of them. Therefore, the faster velocity of injection of the Agar solutions can increase the pore saturation in the air and clean the more contaminated liquid in the soil, regardless of the concentration of the Agar solutions.

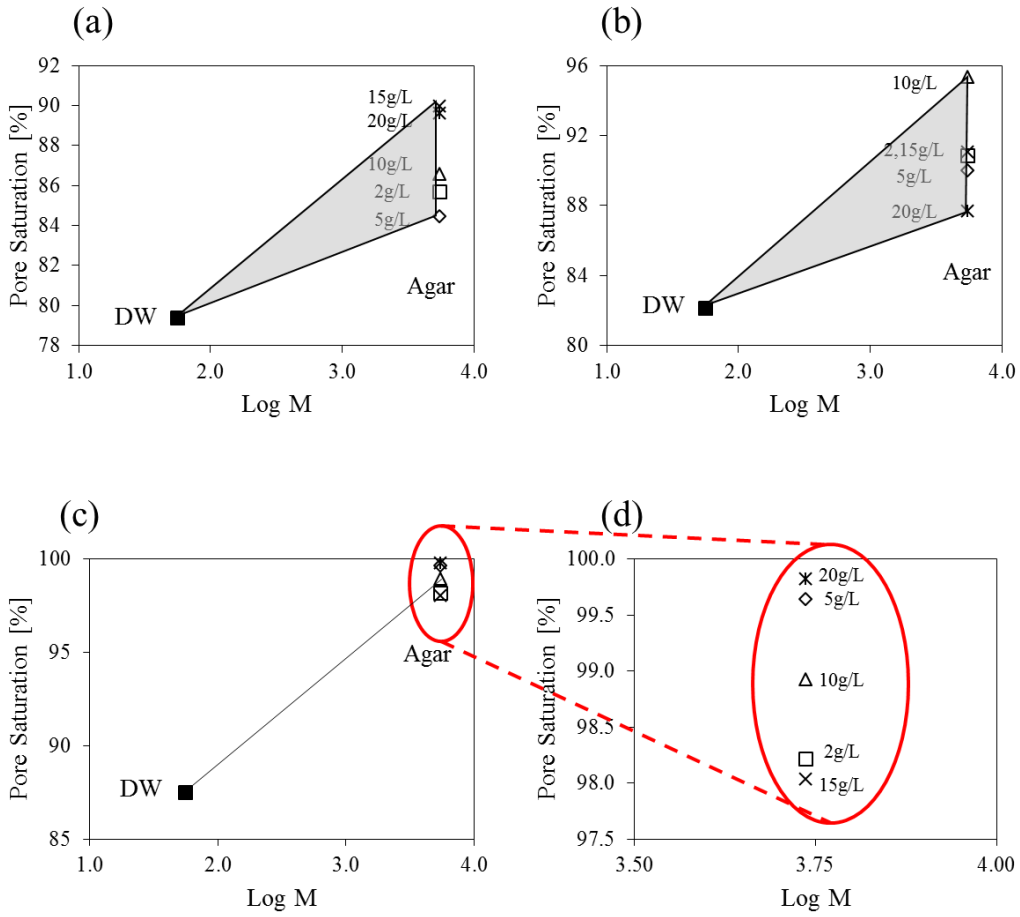

Figure 5.1. The correlation between pore saturation and Log M (mobility ratio) of Agar solutions (2, 5, 10, 15, 20g/L) at room temperature (25℃) in the air. (a) 0.3µl/min. (b) 1.0µl/min. (c) 50µl/min. (d) 50µl/min in details.

Figure 5.2 illustrates how the capillary number (C) of Agar solutions (2, 5, 10, 15, 20g/L) and distilled water (0g/L) affects pore saturation with three different flow rates (0.3, 1.0, 50µl/min) by their increments at the same temperature (25°). These results is very similar, compare to Fig 5.1. With increments of Log C (Capillary number), pore saturations of the Agar solutions are usually higher than ones of distilled water. The higher concentration of the Agar solutions has no relationship through 5.2 (a), (b), and (c). There is no correlation between the concentration and flow rate of the Agar solutions.

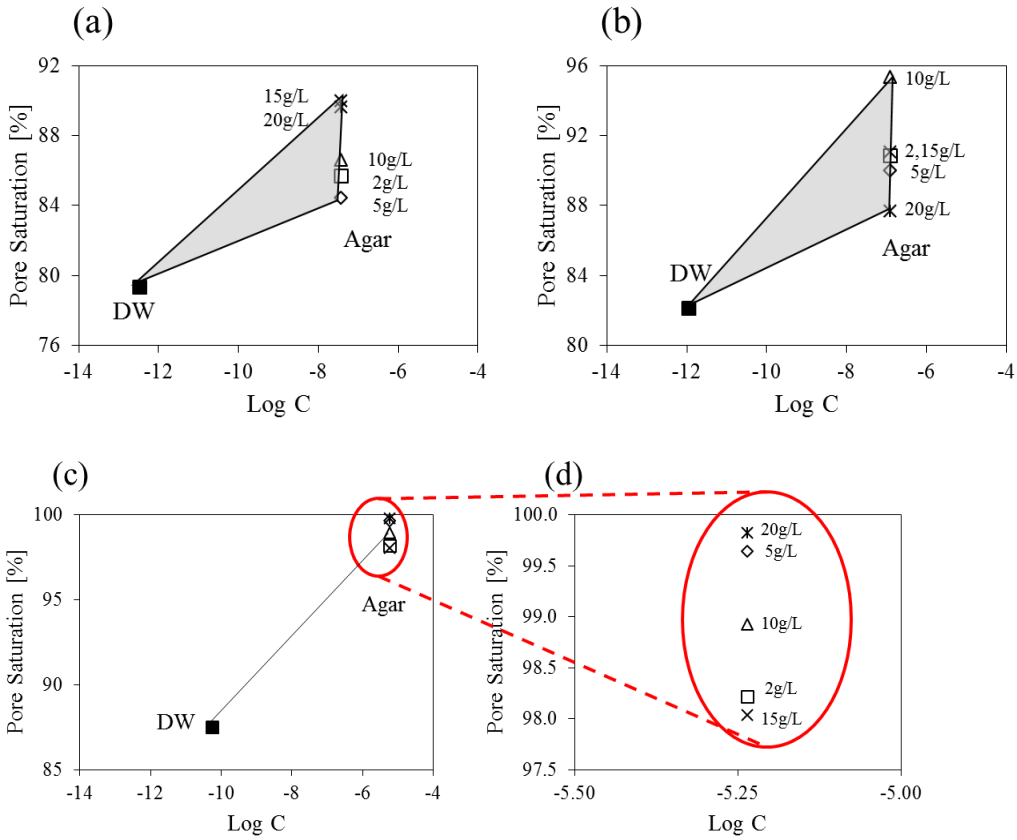

Figure 5.2. The correlation between pore saturation and Log C (Capillary number) of Agar solutions (2, 5, 10, 15, 20g/L) at room temperature (25℃) in the air. (a) 0.3μl/min. (b) 1.0μl/min. (c) 50μl/min. (d) 50μl/min in details.

The log M – C plot of the Agar solutions in the air is shown in Fig 5.3. The mobility ratio of the Agar solutions is the same due to the assumption of the same viscosity of Agar, regardless of its concentration. The value of Log M of Agar is 3.737 in the air, and the results of Log C of Agar are -7.443 (0.3μl/min), -6.920 (1μl/min), and -5.236 (50μl/min). This means that faster injecting velocities can increase the capillary number. Therefore, the displacement aspects of the Agar solutions may change from capillary fingering to stable displacement if the injecting velocity of Agar solutions is higher than 50μl/min (Lenormand 1990; Ewing and Berkowitz 2001).

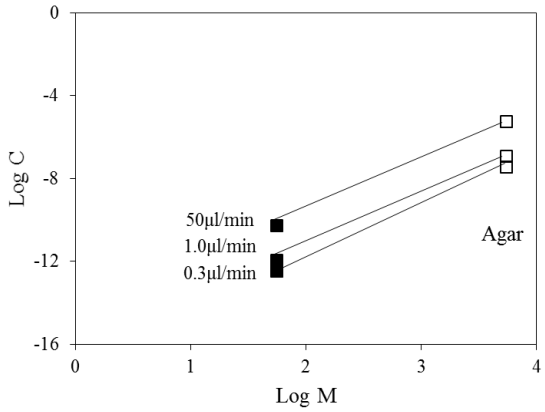

Figure 5.3. The correlation between the mobility ratio (M) and the Capillary number (C) of distilled water and Agar solutions (2, 5, 10, 15, 20g/L) at room temperature (25℃) in the air.
*The viscosity of all Agar solutions is assumed as the one of 0.2g/L Agar solution. Therefore, the results of Agar solutions in the log M – C plane are the same.

The results of Log M of the PAM solutions are similar when compared with the Agar solutions shown in Fig 5.4 (a). The results of Log C for the PAM solutions are a somewhat linear with pore saturation. However, the concentration of the PAM solutions is almost unrelated for pore saturation shown in Fig 5.4 (b).

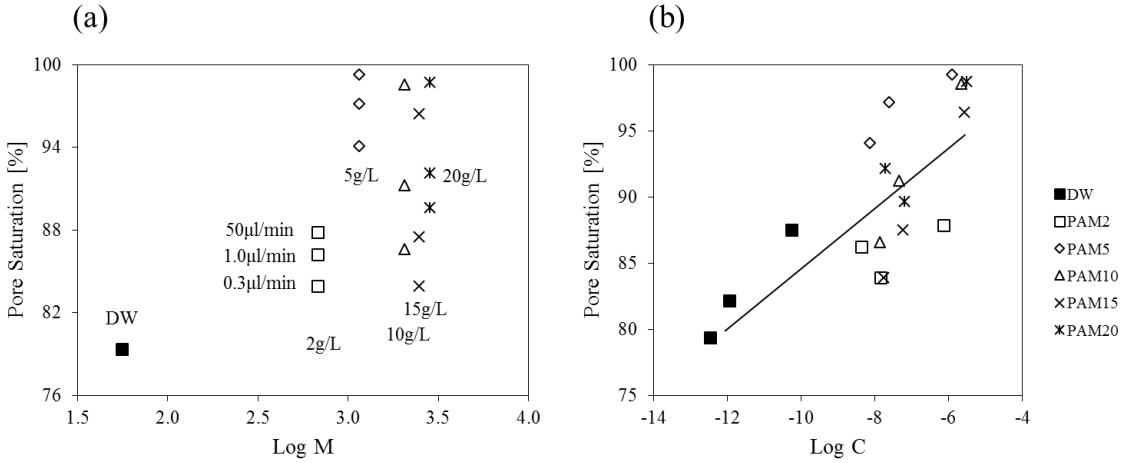

Figure 5.4. The correlation between pore saturation and (a) the mobility ratio (M) and (b) the capillary number (C) of distilled water and PAM solutions (2, 5, 10, 15, 20g/L) at room temperature (25℃) in the air.

The Log M – C plot of the PAM solutions show the flow rate and concentration of the PAM solutions. The higher the concentration of the PAM solutions has a larger value of Log M (Mobility Ratio), but among the various concentrations of the PAM solutions are very similar for Log C (Capillary Number). When the faster flow rates of PAM solutions inject, the capillary number (C) should be increased, particularly in the flow rate of 50µl/min. That is, increasing flow rate can make it to closer to stable displacement as the equation of capillary number (c) (Lenormand 1990). Moreover, in the air, the trend of the Agar and PAM solutions for C and M has no distinguished characteristics.

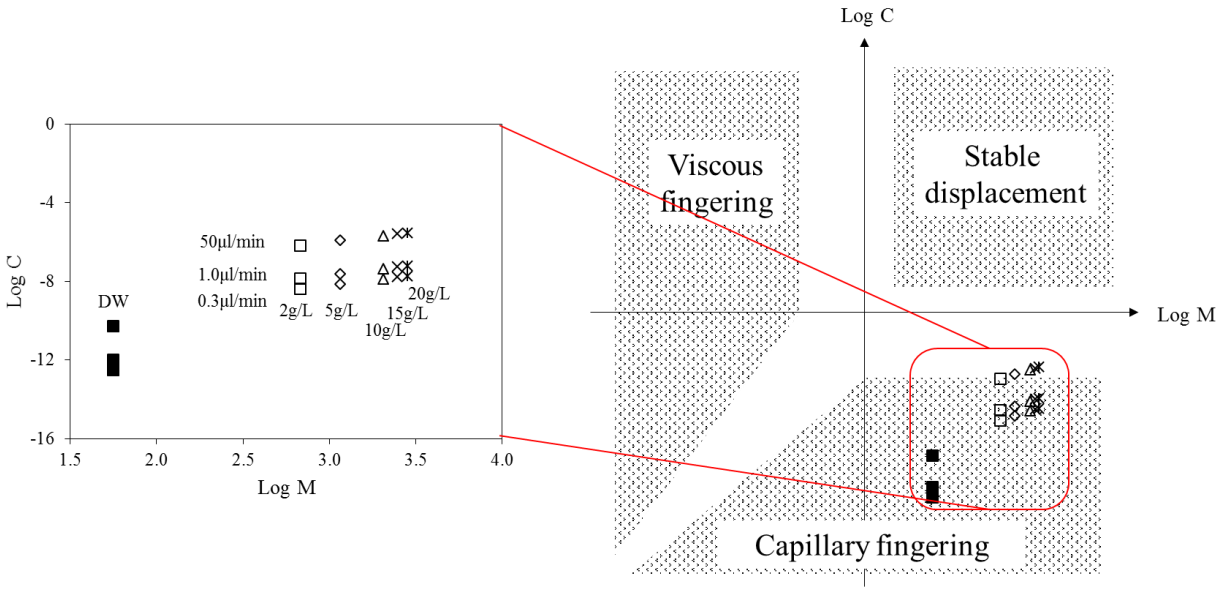

Figure 5.5. The correlation between the mobility ratio (M) and the Capillary number (C) of distilled water and PAM solutions (2, 5, 10, 15, 20g/L) at room temperature (25℃) in the air.

PAM solutions have distinct characteristic in Fig 5.6. Even though higher concentration of PAM solutions is not related to the results of Fig 5.5 in the air, a separate trend line can explain the relationship between the capillary number (C) and mobility ratio (M). That is; the increment of mobility rate (M) can gradually increase the capillary number (C).

Each different concentration of the PAM solutions has a similar tendency for the same mobility ratio, which is the order of the mobility ratio (M) shown in Fig 5.6 (a), at the flow rate of 5.0μl/min, 1.0μl/min, and 0.3μl/min, respectively. On the other hand, the capillary number (C) of the PAM solutions has no tendency.

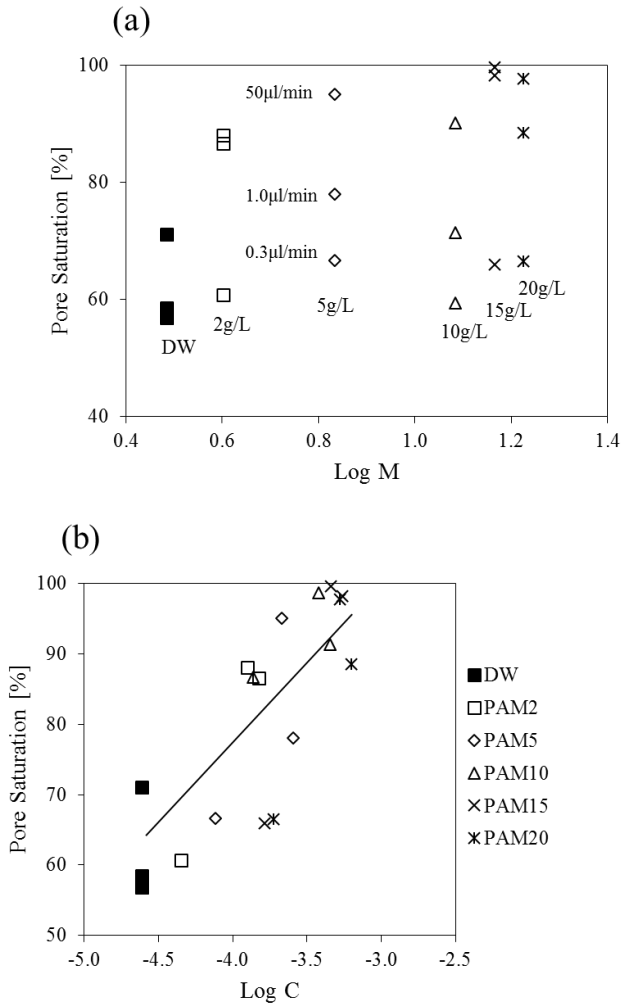

Figure 5.6. The correlation between pore saturation of various PAM solutions in the hexadecane as a function of (a) Mobility ratio (M) and (b) Capillary number (C).

The Log M – C plot of the PAM solutions in the hexadecane (assumed an oil reservoir) have a definite trend. All the PAM solutions with different concentrations and flow rates are located in the transition region (Lenormand 1990; Ewing and Berkowitz 2001). Additionally, as the

concentration of the PAM solutions is increased, their trend is linear along the increment of Log C (capillary number).

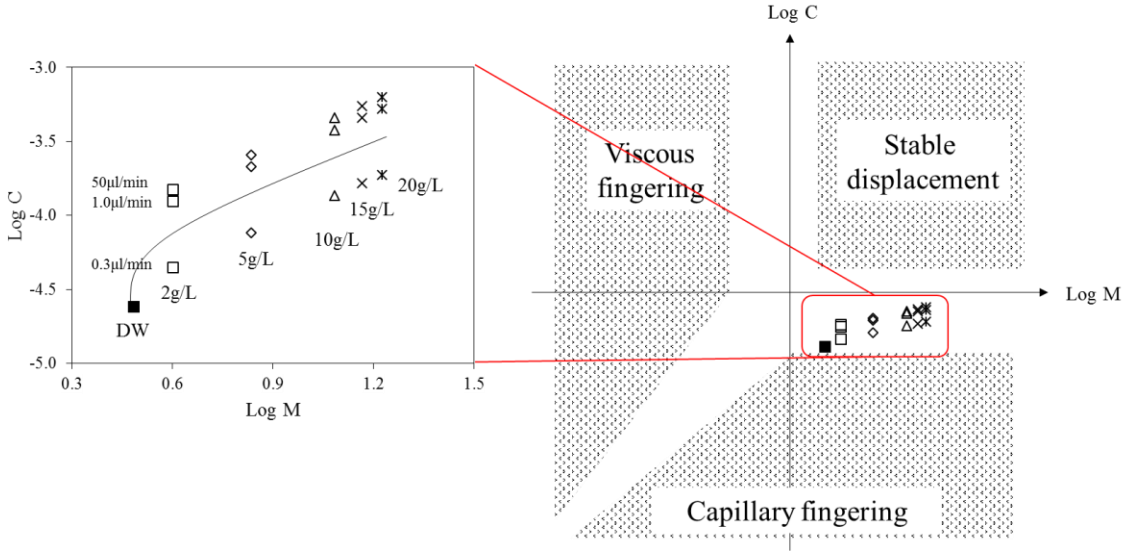

Figure 5.7. Correlation of PAM solutions with a different concentration of the mobility ratio (M) and the Capillary number (C) at room temperature in the hexadecane.

5.2. Estimate of Capillary Pressure using *e, Cc, and Ss*

We have obtained a large amount of results using an experimental test and a theoretical basis. Due to the importance of capillary pressure to understand SWCC, the estimation of capillary pressure is useful for applications in the geotechnical field. In order to estimate capillary pressure, we need specific parameters such as void ratio, e, the concrete surface, S, and the mass density of the mineral, ρ, using the following equation (5.1) (Espinoza and Santamarina 2010):

$$\boldsymbol{Pc = \psi \frac{Ss\ \rho\ \sigma\ cos\theta}{e1kPa - Cc \log \frac{p'}{1kPa}}} \quad (5.1)$$

Where ψ = 4/ (k10$^{\alpha\sigma}$) is usually between 0.04 and 0.08 and *Ss* is the specific surface m^2/kg. ρ is density, kg/m^3 and θ is contact angle, degrees, and σ is interfacial tension, mN/m. Cc is the

compressibility coefficient of the sediment, and p is effective stress (Phadnis and Santamarina 2011; Espinoza and Santamarina 2010). The denominator of the equation (5.1) means that the void ratio can increase when the compressibility coefficient or effective stress is increased. However, increasing the void ratio decreases the capillary pressure. In addition, the concrete surface (Cc), the density (ρ), the contact angle (θ), and interfacial tension (σ) can increase the capillary pressure with their increments.

5.3. Effective Stress on the Capillary Pressure

Using equation (5.1), we have obtained the various sediments shown in Fig 5.8. The smaller pores at the same effective stress are higher than, the larger pores such as silt. Each clay mineralogy has slightly similar tendencies. The range of capillary pressures for silt is subtle and has no differences (3.44 ~ 3.56 Pa) when using the average value of constitutive parameters. The variation of capillary pressure for Kaolinite (92 ~ 134) is slightly larger than silt. At the Illite and Montmorillonite, such a difference is much greater than previous ones.

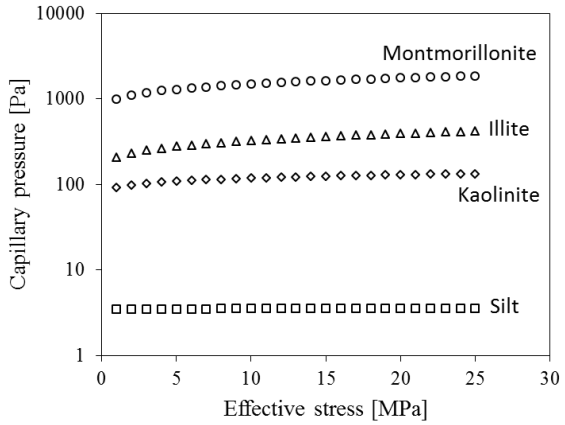

Figure 5.8. Capillary pressure in sediments as a function of depth for different sediment mineralogies using each average values: Silt (e_{100} = 0.7, Cc = 0.06, Ss = 0.5225m^2/g), Kaolinite (e_{100} = 1.0, Cc = 0.3, Ss = 15m^2/g), Illite (e_{100} = 2.5, Cc = 0.8, Ss = 82.5m^2/g), Montmorillonite (e_{100} = 3.25, Cc = 1.5, Ss = 540m^2/g).

Each sediment is shown in Fig 5.9. The capillary pressures (0.32 ~ 7.35 Pa) of silt are almost constant regardless of effective stress. The range of capillary pressures of Illite and Kaolinite are 61 ~ 178 Pa and 163 ~ 511 Pa, respectively. Lastly, Montmorillonite, has the smallest pores (553 ~ 2692 Pa). This means that the smaller sediment is more susceptible to the increment of effective stress shown in Fig 5.9.

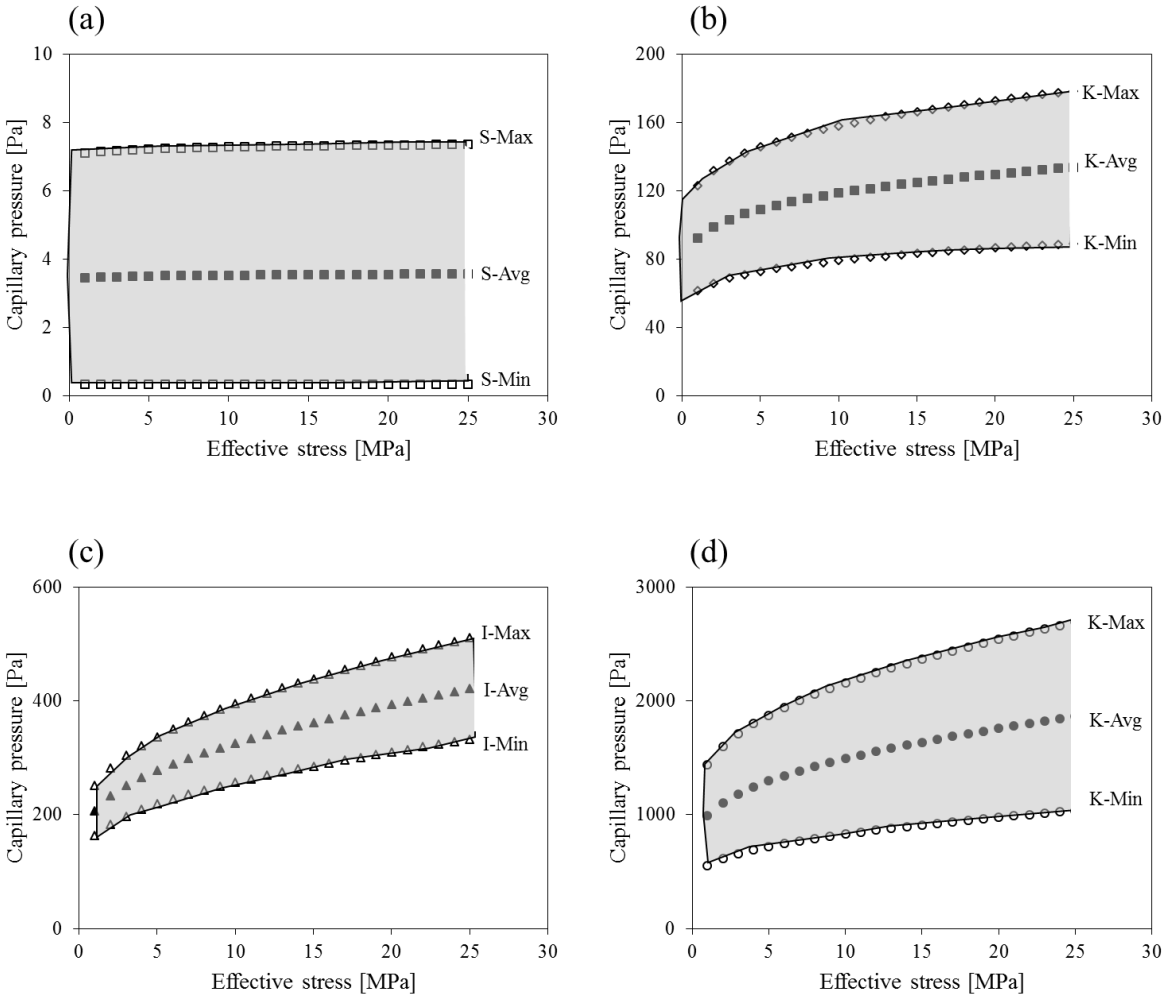

Figure 5.9. Estimate of capillary pressure (Max, Average, Min) in sediments as a function of effective stress (MPa) for different sediment mineralogies: (a) Silt (e_{100} = 0.6 – 0.8, Cc = 0.02 * 0.09, Ss = 0.05 – 1.0 m^2/g), (b) Kaolinite (e_{100} = 0.9 – 1.1, Cc = 0.2 – 0.4, Ss = 10 -20m^2/g), (c) Illite (e_{100} = 2 - 3, Cc = 0.8 - 80, Ss = 65 - 100m^2/g), (d) Montmorillonite (e_{100} = 3.25, Cc = 1.5, Ss = 300 - 780m^2/g).

CHAPTER 6. CONCLUSIONS AND FUTURE WORK

6.1. Conclusions

The ultimate goal of this paper is to characterize biopolymers (Agar and PAM) and their implication on EOR. In order to evaluate them, viscosity, contact angle, and surface tension tests are conducted to discover the fundamental properties of biopolymers. Their flow characteristic in porous media is investigated by Microfluidic models and SWCC tests. We draw definite conclusions:

1. Through the results of the viscosity test, 0.2g/L Agar has the highest viscosity compared to the other solutions. The viscosity of the PAM solutions has a slight difference with the increase of the concentration of PAM, but the viscosity of each PAM solution with the increment of temperature is decreased.
2. Contact angles of biopolymers increase as their higher concentration in the air, and they are greater than the contact angles of viscosity. However, contact angles of Agar solutions into an oil reservoir assumed as the hexadecane are an inverse trend. Contact angles of PAM solutions have no tendency in the hexadecane.
3. The surface tension of biopolymers (63.3 ~ 65.1 mN/m) are mostly smaller than distilled water (72mN/m).
4. The pore saturation of the PAM solutions is always greater than distilled water in the hexadecane using Microfluidic models. The faster injecting velocity of PAM solutions is, of course, possible to improve sweep efficiency, pore saturation. However, a higher

concentration of the PAM solutions has no relationship between concentration and pore saturation.

5. The capillary pressure of distilled water is about 32 ~35 cm H_2O, but the 2g/L PAM solution is approximately 75 cm H_2O. Putting the PAM solution into the ground needs higher capillary pressure and then it starts to dry at over 75 cm H_2O.
6. The application of the Agar and PAM solutions in the air increase pore saturation, compared to distilled water. In an oil reservoir, PAM solutions can quickly sweep the residual oil if their flow rate increases.
7. The smaller sediments are susceptible, compared with silt. The variation of the capillary pressure of Montmorillonite is much greater than other sediments such as Illite, Kaolinite, and Silt.

6.2. Future Work

The results of this study have characterized biopolymers (Agar and PAM) and imply their application to EOR techniques. Nevertheless, some suggestions are given.

1. The viscosity of the 2, 5, 10, 15, 20g/L Agar solutions will be measured using a computer to obtain continuous results. The surface tension of the Agar and PAM solutions will be conducted using a computer as well.
2. The lower Agar solutions will be tested using Microfluidic models. The testing will be carried out to obtain the results of pore saturation of Agar and PAM solutions with various flow rates. The SWCC testing will be performed using the Agar solutions and the rest of the PAM solutions (5, 10, 15, 20g/L).

REFERENCES

Abdelrahim, M. (2012). "Measurement of interfacial tension in hydrocarbon/water/dispersant systems at deepwater conditions." Faculty of the Louisiana State University and Agricultural and Mechanical College in partial fulfillment of the requirements for the degree of Master of Science in Petroleum Engineering In The Craft & Hawkins Department of Petroleum Engineering by Mohamed Abdelrahim BS in Petroleum Engineering, Louisiana State University.

Alvarado, V., and Manrique, E. (2010). "Enhanced oil recovery: an update review." *Energies*, 3(9), 1529-1575.

Armisen, R., and Galatas, F. (1987). "Production, properties and uses of agar." *Production and utilization of products from commercial seaweeds. FAO Fish. Tech. Pap*, 288, 1-57.

Barvenik, F. W. (1994). "Polyacrylamide characteristics related to soil applications." *Soil Science*, 158(4), 235-243.

Bornman, J., and Barnard, R. (1993). "The possible use of agar gel in plant nutritional studies." *South African Journal of Plant and Soil*, 10(3), 146-149.

Busscher, W., Bjorneberg, D., and Sojka, R. (2009). *"Field application of PAM as an amendment in deep-tilled US southeastern coastal plain soils." Soil and Tillage Research, 104(2), 215-220.*

Chandra, R., and Rustgi, R. (1998). "Biodegradable polymers." *Progress in polymer science*, 23(7), 1273-1335.

Chen, J. (2003). "Rheology and machining performance of waterborne biopolymer labelling adhesives." *Journal of adhesion science and technology*, 17(3), 409-421.

Choo, H. (2013). "Engineering behavior and characterization of physical-chemical particulate mixtures using geophysical measurement techniques."

Comba, S., and Sethi, R. (2009). "Stabilization of highly concentrated suspensions of iron nanoparticles using shear-thinning gels of xanthan gum." *Water research*, 43(15), 3717-3726.

Cyber Colloids (2015). "Introduction to Agar-Structure." Retrieved Feb, 25, 2015 from http://www.cybercolloids.net/information/technical-articles/introduction-agar-structure.

Das, B. M. (2005). "Fundamentals of Geotechnical Engineering."

Dimitrov, A., Kralchevsky, P., Nikolov, A., Noshi, H., and Matsumoto, M. (1991). "Contact angle measurements with sessile drops and bubbles." *Journal of colloid and interface science*, 145(1), 279-282.

Du, Y., Zhang, G., Ge, J., Li, G., and Feng, A. (2013). "Influence of Oil Viscosity on Alkaline Flooding for Enhanced Heavy Oil Recovery." *Journal of Chemistry*, 2013.

Dukhin, A. S., and Goetz, P. J. (2009). "Bulk viscosity and compressibility measurement using acoustic spectroscopy." *The Journal of chemical physics*, 130(12), 124519.

Elert, G. (1998). "Viscosity." *The Physics Hypertextbook*, 2014.

Erkekoglu, P., and Baydar, T. (2014). "Acrylamide neurotoxicity." *Nutritional neuroscience*, 17(2), 49-57.

Espinoza, D. N., and Santamarina, J. C. (2010). "Water-CO2-mineral systems: Interfacial tension, contact angle, and diffusion—Implications to CO2 geological storage." *Water resources research*, 46(7).

Ewing, R. P., and Berkowitz, B. (2001). "Stochastic pore-scale growth models of DNAPL migration in porous media." Advances in water resources, 24(3), 309-323.

Fimmtech (2007). "Polymer Viscosity." Retrieved 2007 from

http://www.injectionmoldingonline.com/Molding101/PolymerViscosity.aspx.

Fredlund, D. (1995). "Prediction of Unsaturated Soil Functions Using the Soil-Water Characteristic Curve." *GEOTECHNICAL ENGINEERING*, 13, 16.

Fredlund, D. G., and Morgenstern, N. R. (1977). "Stress state variables for unsaturated soils." *Journal of Geotechnical and Geoenvironmental Engineering*, 103(ASCE 12919).

Fredlund, D. G., and Rahardjo, H. (1993). *Soil mechanics for unsaturated soils*, John Wiley & Sons.

Fredlund, D. G., Rahardjo, H., and Fredlund, M. D. (2012). Unsaturated soil mechanics in engineering practice, John Wiley & Sons.

Fredlund, D. G., and Xing, A. (1994). "Equations for the soil-water characteristic curve." *Canadian geotechnical journal*, 31(4), 521-532.

Freile-Pelegrín, Y., Madera-Santana, T., Robledo, D., Veleva, L., Quintana, P., and Azamar, J. (2007). "Degradation of agar films in a humid tropical climate: Thermal, mechanical, morphological and structural changes." *Polymer Degradation and Stability*, 92(2), 244-252.

Han, T., Xu, G., Chen, Y., Zhou, T., Tan, Y., Lv, X., and Zhang, J. (2012). "Improving performances of hydrophobically modified polyacrylamide in mineralized water by block polyether with branched structure." *Journal of Dispersion Science and Technology*, 33(5), 697-703.

Hardy, R. C., and Cottington, R. L. (1949). "Viscosity of deuterium oxide and water in the range of 5 to 125 C." J Res Natl Bureau Standards, 42, 573-578.

Jang, S. S., Lin, S.-T., Maiti, P. K., Blanco, M., Goddard, W. A., Shuler, P., and Tang, Y. (2004). "Molecular dynamics study of a surfactant-mediated decane-water interface: Effect of molecular architecture of alkyl benzene sulfonate." *The Journal of Physical Chemistry B*, 108(32), 12130-12140.

Kang, J., Sowers, T. D., Duckworth, O. W., Amoozegar, A., Heitman, J. L., and McLaughlin, R. A. (2013). "Turbidimetric determination of anionic polyacrylamide in low carbon soil extracts." *Journal of environmental quality*, 42(6), 1902-1907.

Khan, M., and Islam, M. (2007). "Handbook of Petroleum Engineering: Sustainable Operations." *Houston, TX: Gulf Publishing Company*, 461.

Khatami, H. R., and O'Kelly, B. C. (2012). "Improving mechanical properties of sand using biopolymers." *Journal of Geotechnical and Geoenvironmental Engineering*, 139(8), 1402-1406.

Kim, S., and Santamarina, J. C. (2014). "Engineered CO2 injection: The use of surfactants for enhanced sweep efficiency." *International Journal of Greenhouse Gas Control*, 20, 324-332.

Lambe, T., and Whitman, R. (1969). "Soil Mechanics, 553 pp." John Wiley, New York.

Lee, B.-B., Chan, E.-S., Ravindra, P., and Khan, T. A. (2012). "Surface tension of viscous biopolymer solutions measured using the du Nouy ring method and the drop weight methods." *Polymer bulletin*, 69(4), 471-489.

Lenormand, R. (1990). "Liquids in porous media." *Journal of Physics: Condensed Matter*, 2(S), SA79.

Lenormand, R., Touboul, E., and Zarcone, C. (1988). "Numerical models and experiments on immiscible displacements in porous media." *Journal of Fluid Mechanics*, 189, 165-187.

Lentz, R., and Sojka, R. (1994). "Field results using polyacrylamide to manage furrow erosion and infiltration." *Soil Science*, 158(4), 274-282.

Lentz, R. D., and Sojka, R. E. (2009). "Long-term polyacrylamide formulation effects on soil erosion, water infiltration, and yields of furrow-irrigated crops." *Agronomy journal*, 101(2), 305-314.

Lu, N., Kim, T.-H., Sture, S., and Likos, W. J. (2009). "Tensile strength of unsaturated sand." *Journal of engineering mechanics*, 135(12), 1410-1419.

Lu, N., and Likos, W. J. (2004). *Unsaturated soil mechanics*, J. Wiley.

Martin, G., Yen, T., and Karimi, S. (1996). "Application of biopolymer technology in silty soil matrices to form impervious barriers."

Moseley, W. A., and Dhir, V. K. (1996). "Capillary pressure-saturation relations in porous media including the effect of wettability." *Journal of hydrology*, 178(1), 33-53.

Phadnis, H., and Santamarina, J. (2011). "Bacteria in sediments: pore size effects." *Geotechnique Letters*, 1(October-December), 91-93.

Praiboon, J., Chirapart, A., Akakabe, Y., Bhumibhamond, O., and Kajiwara, T. (2006). "Physical and chemical characterization of agar polysaccharides extracted from the Thai and Japanese species of Gracilaria." *Sci Asia*, 32(Suppl 1), 11-17.

Rahman, P. K., Pasirayi, G., Auger, V., and Ali, Z. (2010). "Production of rhamnolipid biosurfactants by Pseudomonas aeruginosa DS10-129 in a microfluidic bioreactor." *Biotechnology and applied biochemistry*, 55(1), 45-52.

Romero-Zerón, L. (2012). *Advances in Enhanced Oil Recovery Processes*, INTECH Open Access Publisher.

Ryan, B. J., and Poduska, K. M. (2008). "Roughness effects on contact angle measurements." *American Journal of Physics*, 76(11), 1074-1077.

Sakaki, T., and Illangasekare, T. H. (2007). "Comparison of height-averaged and point-measured capillary pressure–saturation relations for sands using a modified Tempe cell." *Water resources research*, 43(12).

Satyanaga, A., Rahardjo, H., Leong, E.-C., and Wang, J.-Y. (2013). "Water characteristic curve of soil with bimodal grain-size distribution." *Computers and Geotechnics*, 48, 51-61.

Sinha, P. K., and Wang, C.-Y. (2007). "Pore-network modeling of liquid water transport in gas diffusion layer of a polymer electrolyte fuel cell." *Electrochimica Acta*, 52(28), 7936-7945.

Sojka, R., Bjorneberg, D., Entry, J., Lentz, R., and Orts, W. (2007). "Polyacrylamide in agriculture and environmental land management." *Advances in Agronomy*, 92, 75-162.

Sojka, R., Entry, J. A., and Fuhrmann, J. J. (2006). "The influence of high application rates of polyacrylamide on microbial metabolic potential in an agricultural soil." *Applied Soil Ecology*, 32(2), 243-252.

Sojka, R., and Lentz, R. (1997). "Reducing furrow irrigation erosion with polyacrylamide (PAM)." *Journal of Production Agriculture*, 10(1), 47-52.

Sojka, R., and Surapaneni, A. (2000). "Potential use of polyacrylamide (PAM) in Australian agriculture to improve off and on-site environmental impacts and infiltration management."

Spyropoulos, F., Frith, W., Norton, I., Wolf, B., and Pacek, A. (2007). "Morphology and shear viscosity of aqueous two-phase biopolymer-surfactant mixtures." *Journal of Rheology (1978-present)*, 51(5), 867-881.

Standnes, D. C., and Skjevrak, I. (2014). "Literature review of implemented polymer field projects." *Journal of Petroleum Science and Engineering*, 122, 761-775.

Subramanian, R. S. (2002). "Non-Newtonian Flows." *Department of Chemical and Biomolecular Engineering, Clarkson University, http://web2. clarkson. edu/projects/subramanian/ch330/notes/Non-Newtonian% 20Flows. pdf*.

Vargaftik, N., Volkov, B., and Voljak, L. (1983). "International tables of the surface tension of water." *Journal of Physical and Chemical Reference Data*, 12(3), 817-820.

Ver Vers, L. M. (1999). "Determination of acrylamide monomer in polyacrylamide degradation studies by high-performance liquid chromatography." *Journal of chromatographic science*, 37(12), 486-494.

Washburn, E. W. (1921). "The dynamics of capillary flow." *Physical review*, 17(3), 273.

Weisbrod, N., Niemet, M. R., and Selker, J. S. (2002). "Imbibition of saline solutions into dry and prewetted porous media." *Advances in Water Resources*, 25(7), 841-855.

Xue, D., and Sethi, R. (2012). "Viscoelastic gels of guar and xanthan gum mixtures provide long-term stabilization of iron micro-and nanoparticles." *Journal of Nanoparticle Research*, 14(11), 1-14.

Yuan, Y., and Lee, T. R. (2013). "Contact angle and wetting properties." *Surface science techniques*, Springer, 3-34.

Zhu, D., Wei, L., Wang, B., and Feng, Y. (2014). "Aqueous Hybrids of Silica Nanoparticles and Hydrophobically Associating Hydrolyzed Polyacrylamide Used for EOR in High-Temperature and High-Salinity Reservoirs." *Energies*, 7(6), 3858-3871.

APPENDIX A: CONTACT ANGLES OF DISTILLED WATER, AGAR, AND PAM IN THE AIR, HEXADECANE

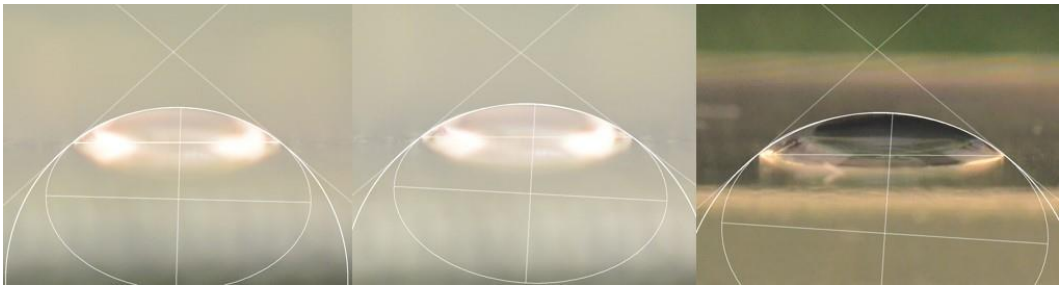

Figure A.1. Analyses of distilled water on contact angle using ImageJ software in the air.

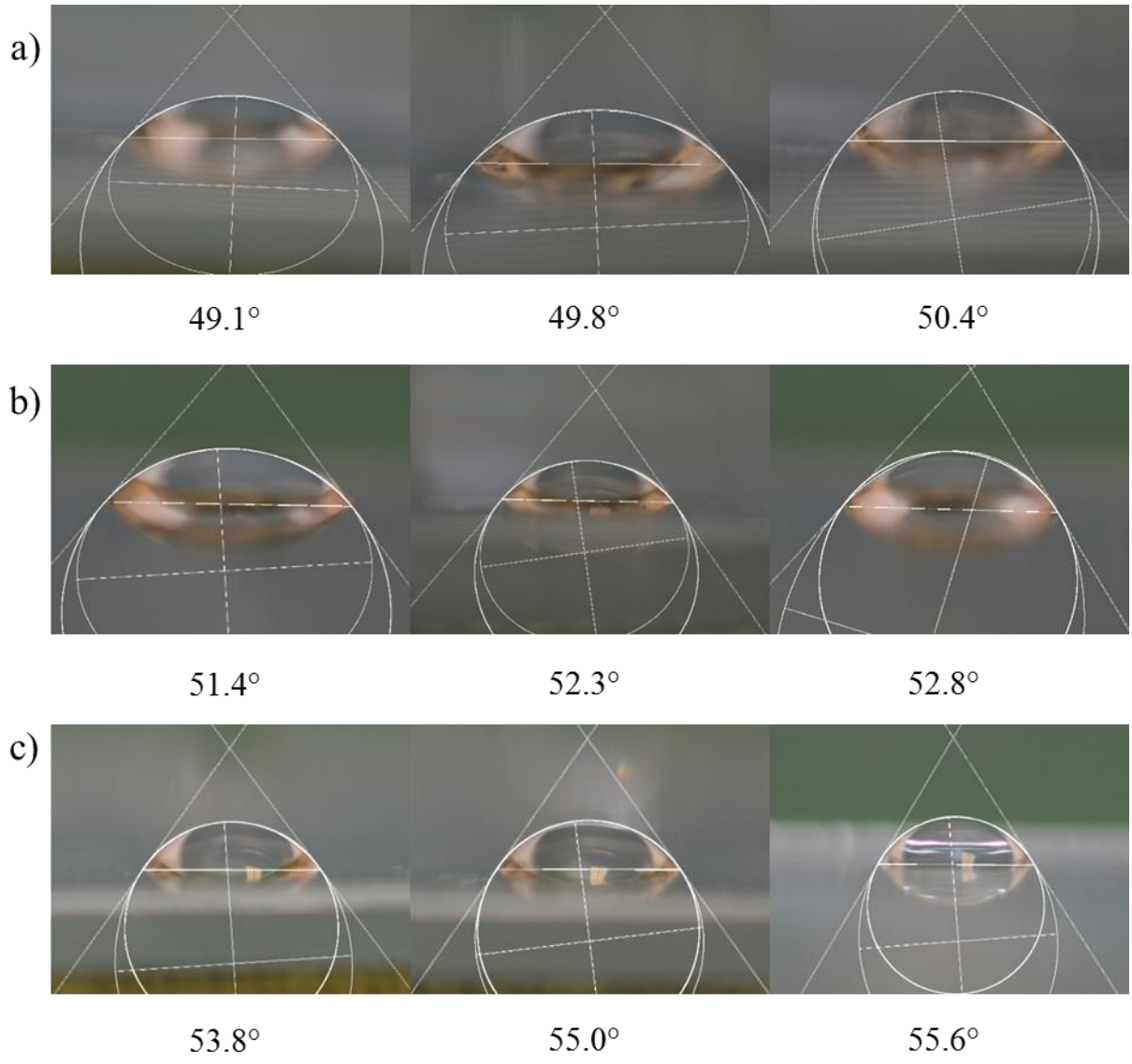

Figure A.2. Analyses of Agar using ImageJ software on contact angle in the air. (a) 2g/L Agar (b) 5g/L Agar (c) 10g/L Agar 15g/L Agar (e) 20g/ /L Agar.

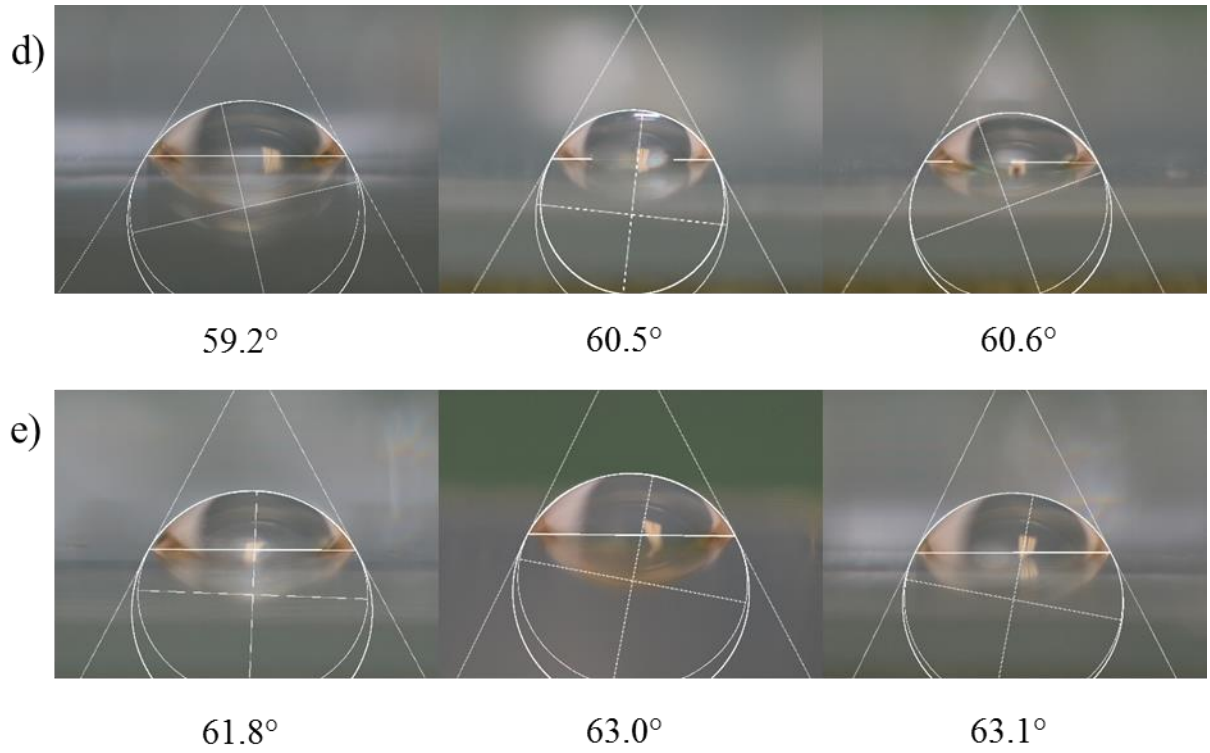

Figure A.2. Continued.

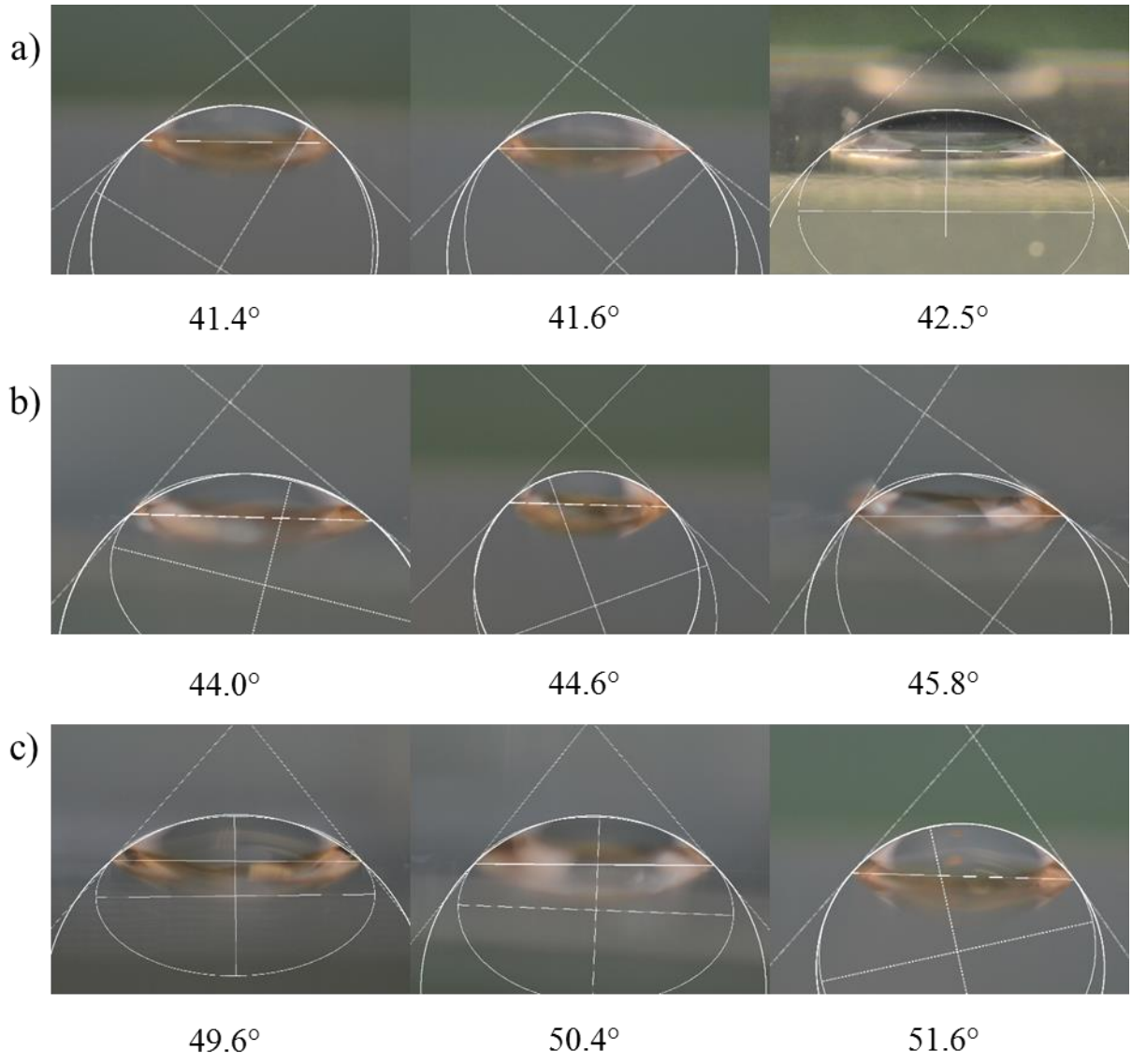

Figure A.3. Analyses of PAM using ImageJ software on contact angle in the air. (a) 2g/L PAM (b) 5g/L PAM (c) 10g/L PAM (d) 15g/L PAM (e) 20g/ /L PAM.

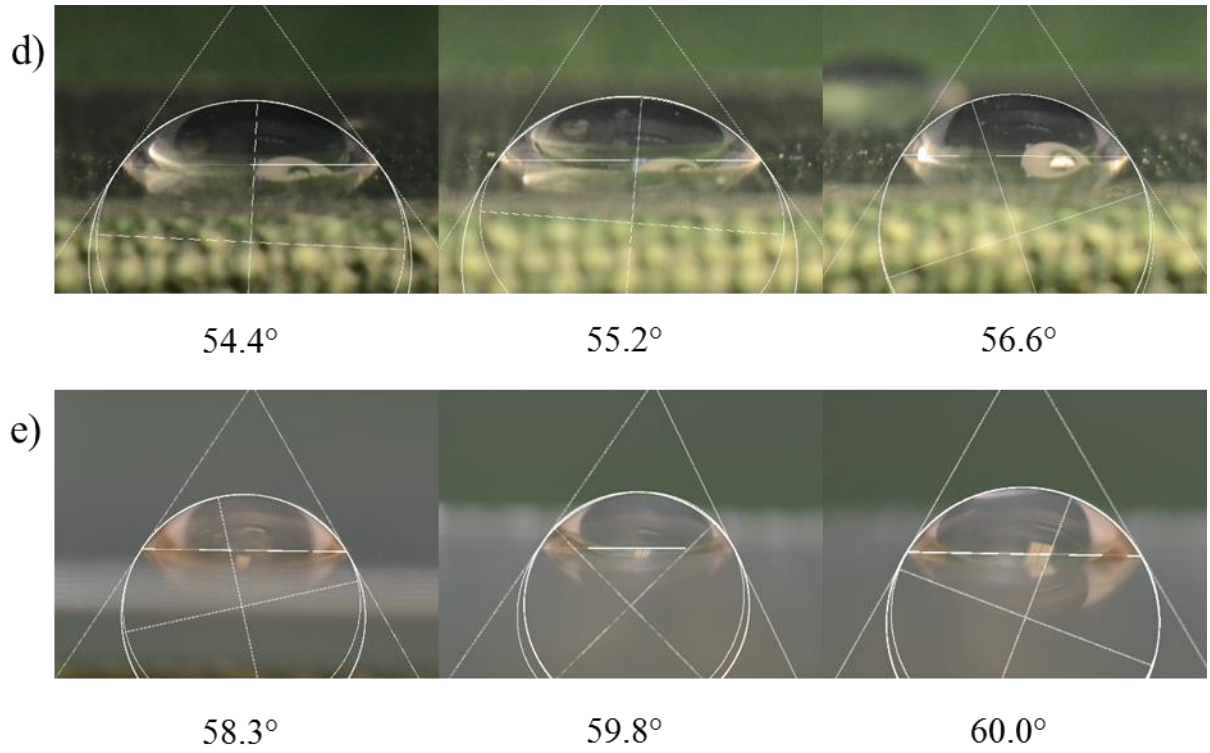

Figure A.3. Continued.

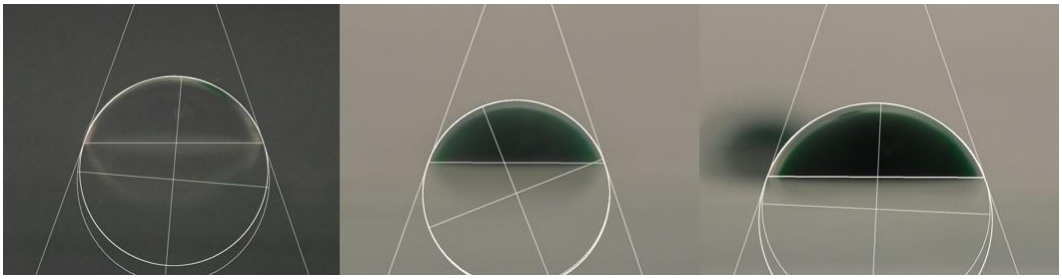

Figure A.4. Analyses of distilled water using ImageJ software on contact angle in the Hexadecane.

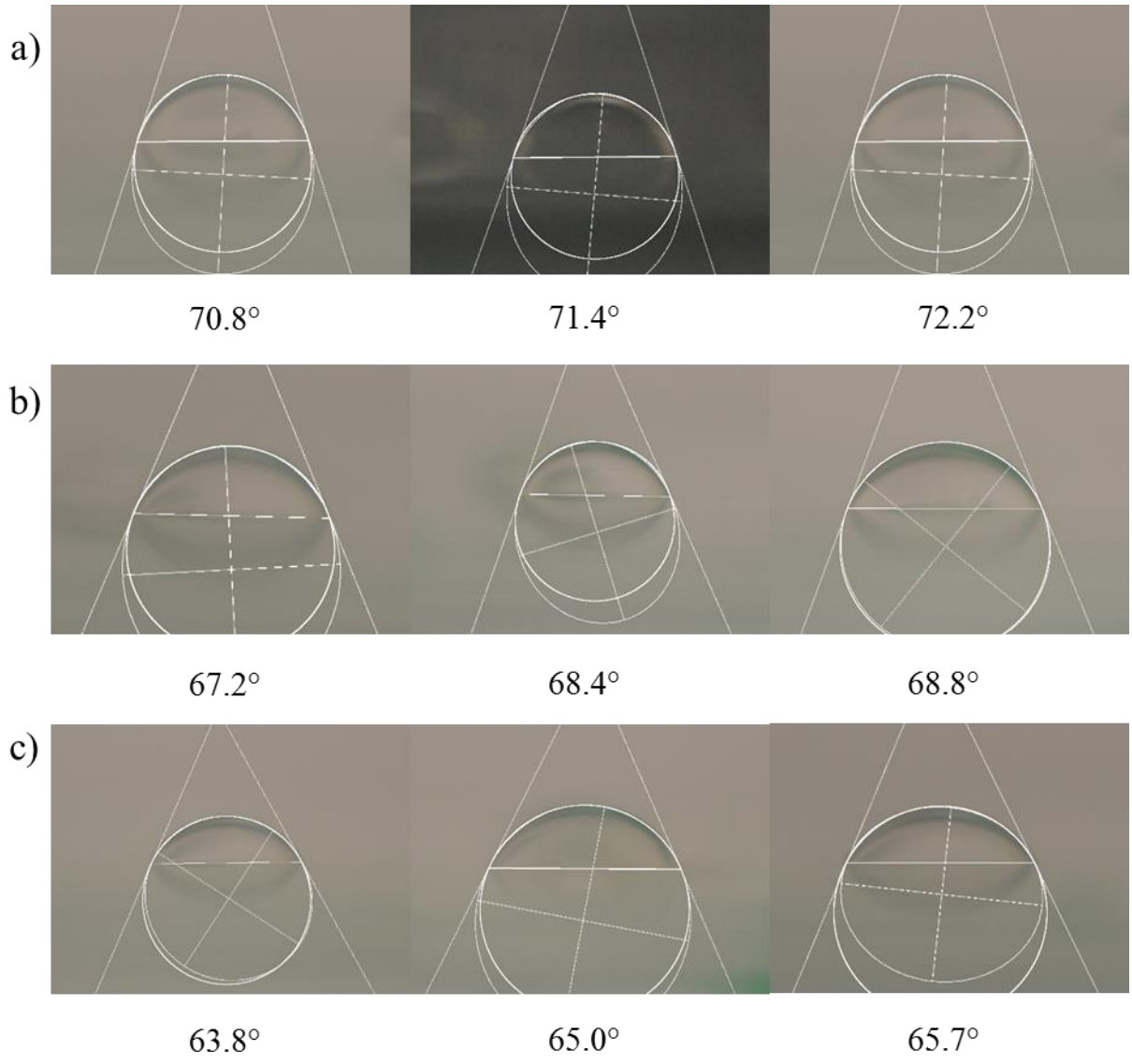

Figure A.5. Analyses of Agar using ImageJ software on contact angle in the Hexadecane. (a) 2g/L Agar (b) 5g/L Agar (c) 10g/L Agar (d) 15g/L Agar (e) 20g/ /L Agar.

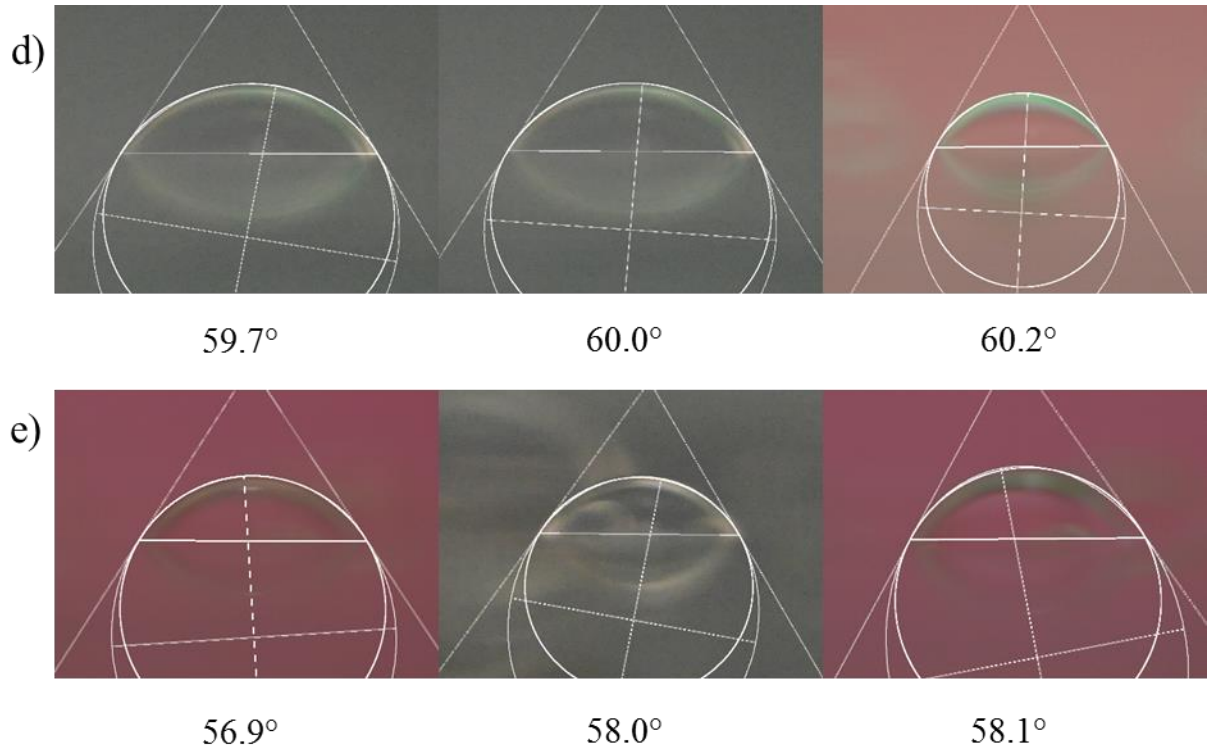

Figure A.5. Continued.

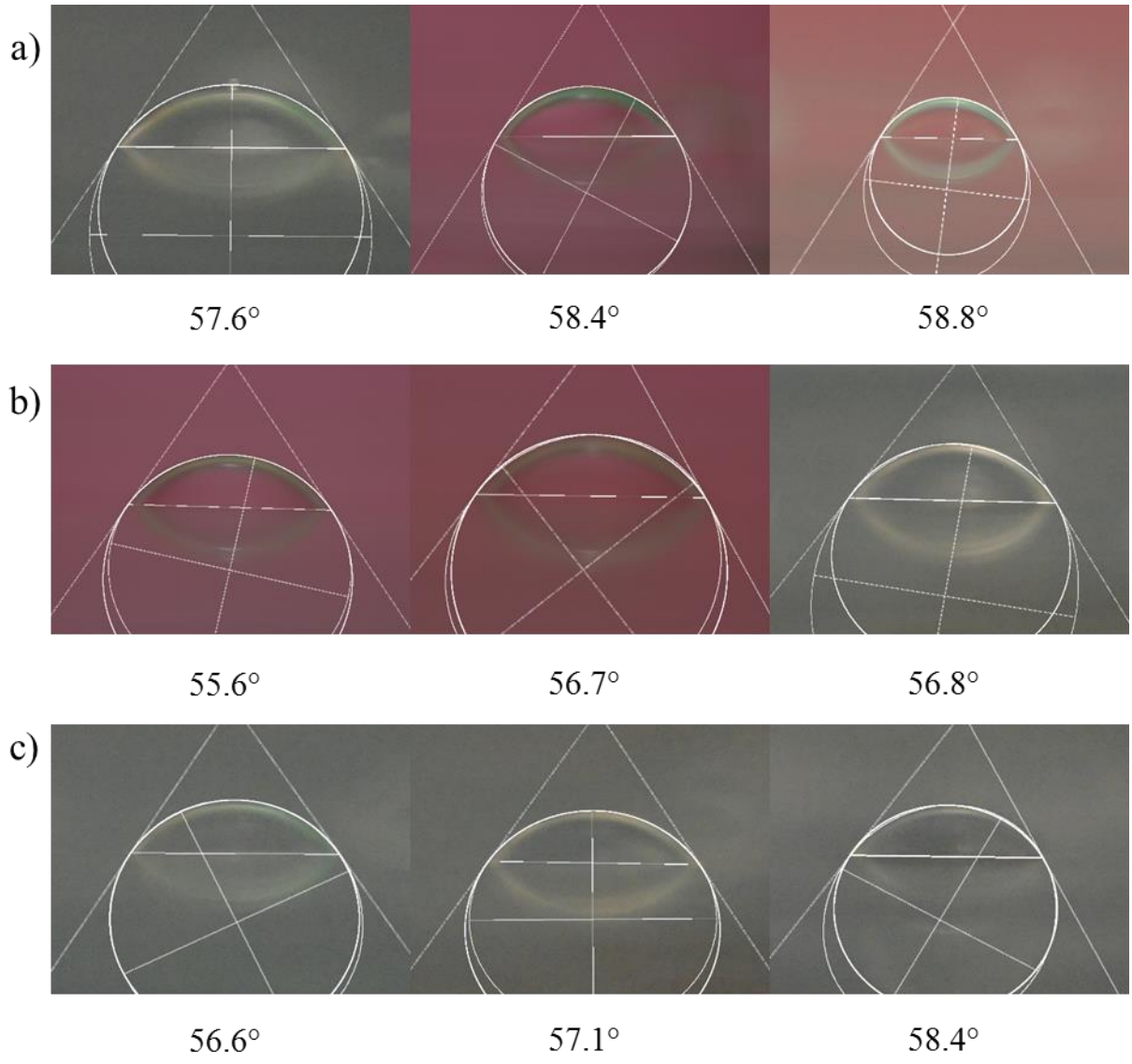

Figure A.6. Analyses of PAM using ImageJ software on contact angle in the Hexadecane. (a) 2g/L PAM (b) 5g/L PAM (c) 10g/L PAM (d) 15g/L PAM (e) 20g/ /L PAM.

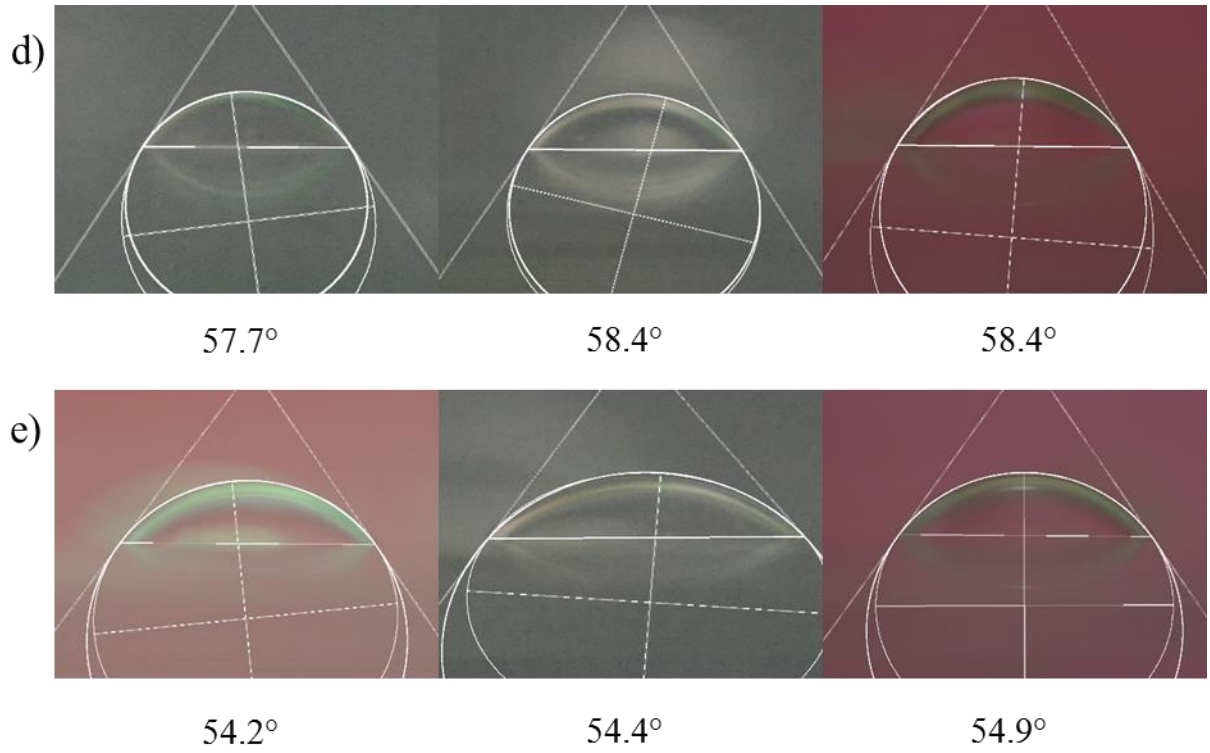

Figure A.6. Continued.

APPENDIX B: THE FLOW PATTERN USING PAM SOLUTIONS IN THE HEXADECANE

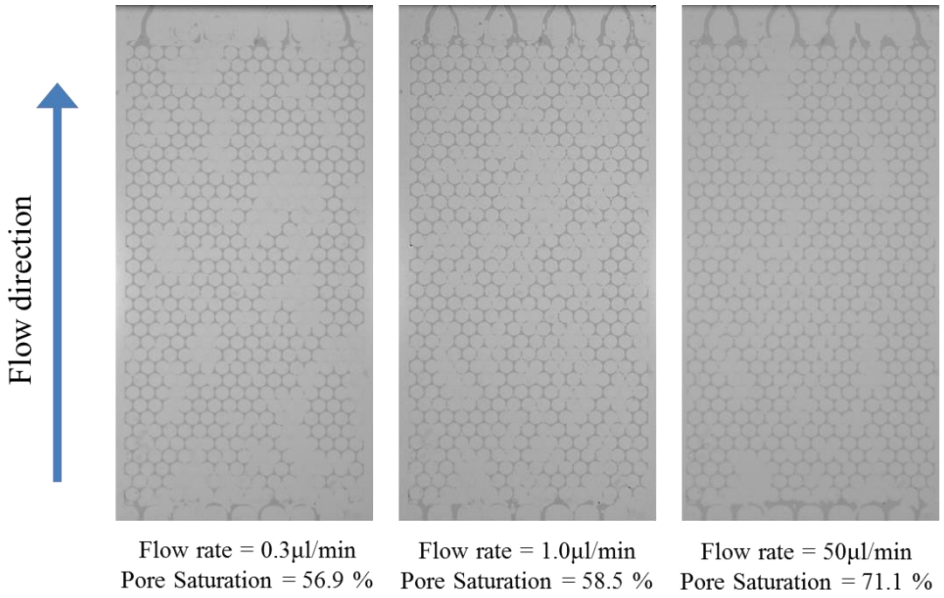

Figure B.1. Displacement patterns of distilled water as a function of the flow rate on Microfluidic models in the Hexadecane.

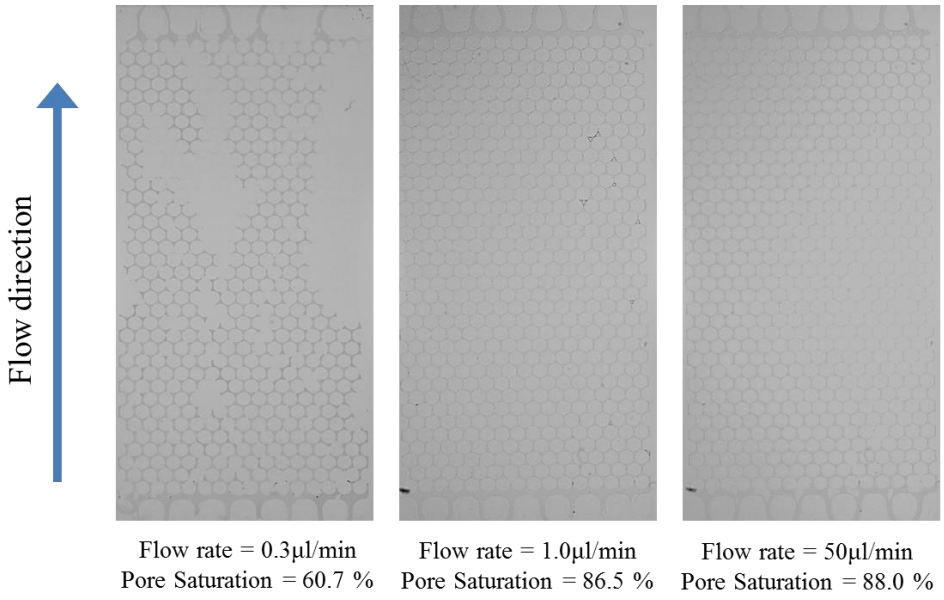

Figure B.2. Displacement patterns of 2g/L PAM as a function of the flow rate on Microfluidic models in the Hexadecane.

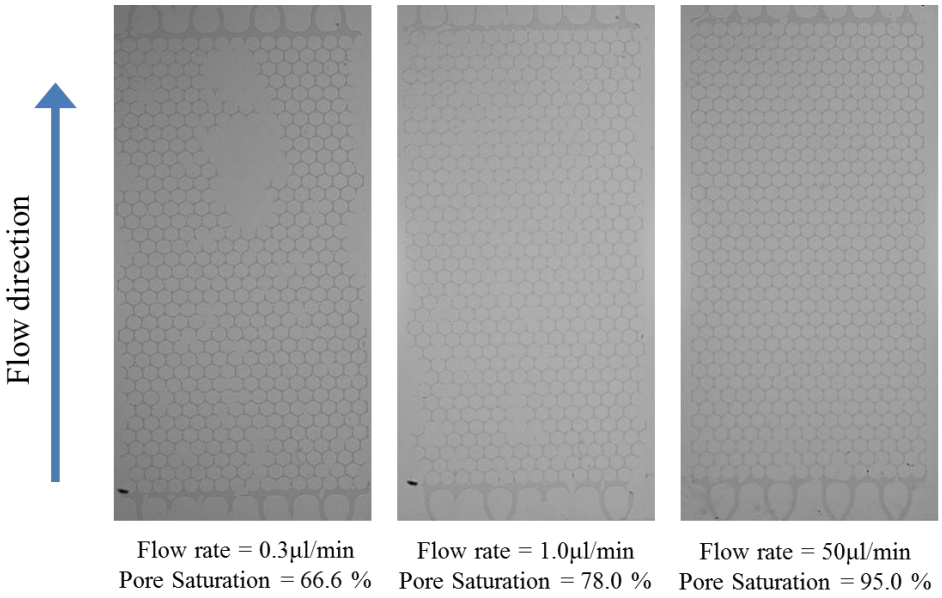

Figure B.3. Displacement patterns of 5g/L PAM as a function of the flow rate on Microfluidic models in the Hexadecane.

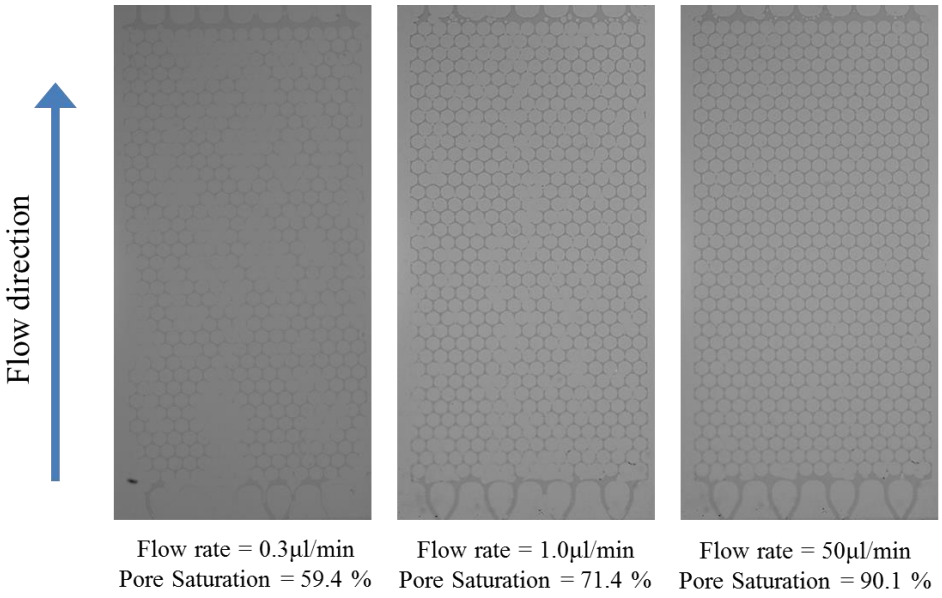

Figure B.4. Displacement patterns of 10g/L PAM as a function of the flow rate on Microfluidic models in the Hexadecane.

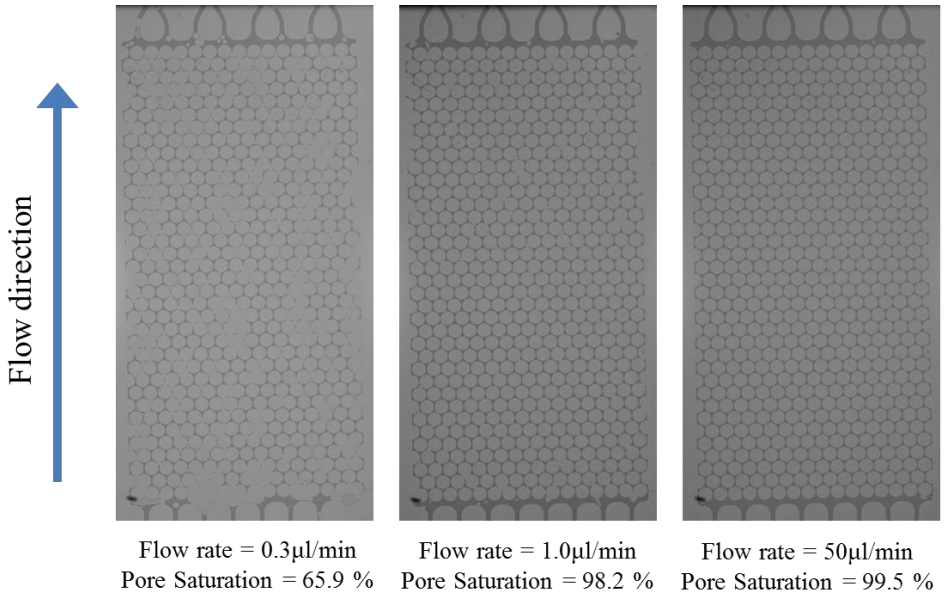

Figure B.5. Displacement patterns of 15g/L PAM as a function of the flow rate on Microfluidic models in the Hexadecane.

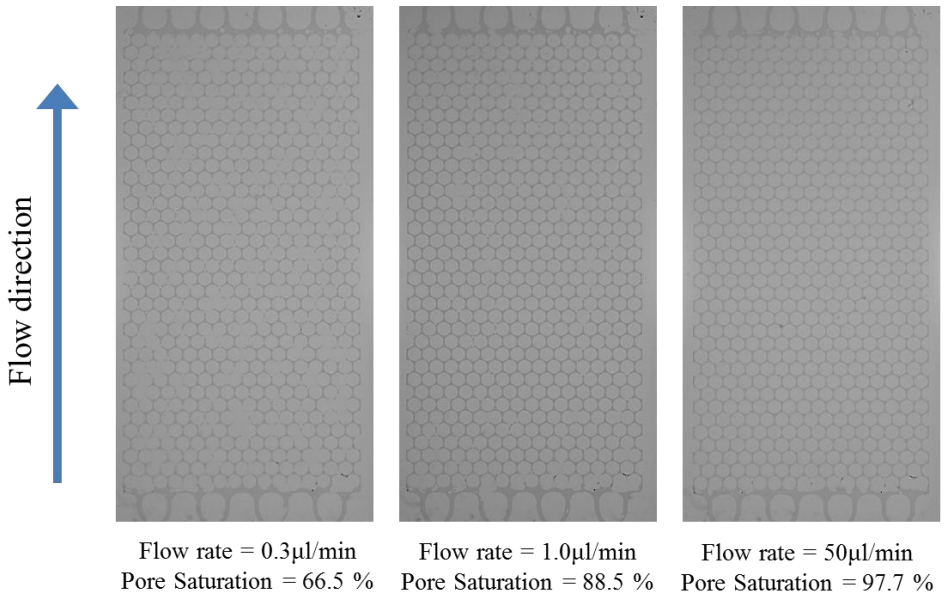

Figure B.6. Displacement patterns of 20g/L PAM as a function of the flow rate on Microfluidic models in the Hexadecane.

VITA

Jungyeon Jang was born in Dongducheon, located in the northern area of South Korea. He attained a Bachelor of Science degree in Civil Engineering from Konkuk University in South Korea in August, 2009. After graduation, he started to work at Donghae Engineering as a civil engineer for two years. After that, he enrolled in the Department of Civil and Environmental Engineering at Louisiana State University (LSU) in 2013. Now, he is eagerly looking forward to receiving a Master's degree, focusing on Geotechnical Engineering, in Civil Engineering at LSU in summer 2015 and then pursuing a Ph.D. program by the following semester.